



# Micromechanical analysis for effective elastic moduli and thermal expansion coefficient of composite materials containing ellipsoidal fillers oriented randomly

Hiroyuki Ono

*Division of Mechanical Engineering, Kyoto Institute of Technology, 1 Matsugasaki, Sakyo-ku, Kyoto City, Kyoto, Japan*



## ARTICLE INFO

**Keywords:**

Effective elastic moduli  
Effective thermal expansion coefficient  
Ellipsoidal filler  
Micromechanics  
Self-consistent method  
Mori-Tanaka method  
Upper and lower bounds

## ABSTRACT

In this study, we examine to derive the solutions of effective elastic moduli and thermal expansion coefficient for composite materials containing ellipsoidal fillers oriented randomly in the material using homogenization theories, which are the self-consistent method and the Mori-Tanaka method. This analysis is carried out by micromechanics combining Eshelby's equivalent inclusion method for each theory. The solutions for effective elastic moduli and thermal expansion coefficient obtained on each theory are expressed by common coefficients composed of both the physical properties of the constituents of the composite material and geometrical factors depending upon the shape of the fillers. Moreover, these solutions enable us to calculate effective elastic moduli and thermal expansion coefficient for composite materials that contain randomly oriented fillers of various shapes and physical properties. By taking the limit of eliminating the existence of the matrix for these solutions, we can derive effective physical properties of polycrystalline materials. Using the obtained solutions, we investigate the effects of the shape of the fillers on the effective elastic moduli and thermal expansion coefficient. As a result, we confirm that these effective properties fall within the lower and upper bounds, and find that a characteristic result appears when the shape of the fillers is flake or oblate. Through comparisons between the analytical and experimental results, we confirm the practical usability of the solutions obtained in this analysis. Furthermore, we determine originally the shape factor for the filler and can show that this factor has the potential to provide guidelines for the optimal design of filler shape to improve the effective elastic properties of materials.

## 1. Introduction

Many industrial products made from composite materials containing fillers are mainly manufactured by setting SMC (sheet molding compound) or BMC (bulk molding compound) into a particular mold and applying pressure and heat. Fillers embedded in composite materials are used as particles, short fibers, and flakes. Such composite materials are molded so that the fillers are oriented two-dimensionally or three-dimensionally and dispersed uniformly in the matrix. The effective properties of such dispersion composites are affected by not only the shape of the fillers but also the distribution of their orientation. Approaches for analyzing the effective physical properties of composite materials can be broadly categorized into numerical methods like the finite element method and theoretical methods based on homogenization theories.

As an example of research based on numerical approaches, Kari et al. evaluated Young's modulus of composite material by generating a unit cell in which fibers were arranged three-dimensionally and analyzing it using a numerical homogenization method based on the finite element method [1]. Wang et al. proposed a complex finite element model for foam materials containing short fibers, in which the shape of the foams is idealized as a tetra decahedron and the fibers are randomly arranged on the walls [2]. El-Abbassi et al. derived the effective Young's modulus of materials containing randomly oriented short fibers in the matrix, by using a specific finite element technique called the Projected Fiber (PF) approach, and compared it with experimental results [3]. Additionally, several studies have analyzed models with a large number of randomly oriented fillers using the finite element method to obtain effective elastic properties of the models [4,5]. However, these analyses require extensive mesh divisions and significant computation time, making it difficult to simultaneously consider filler shape and orientation.

On the other hand, homogenization theories provide alternative approaches, such as the principle of variation [6], the Christensen's method [7,8], the Mori-Tanaka method ([9]), the self-consistent method [10], the differential scheme [11] and so on. The Christensen's method

E-mail address: [hono@kit.ac.jp](mailto:hono@kit.ac.jp).

is an approximate approach that expresses the effective elastic moduli of composite materials containing fibers oriented randomly by using those of composites containing fibers aligned unidirectionally. Huang derived solutions for the effective elastic moduli of composites with randomly oriented spheroidal fillers in two or three dimensions, using the same method as Christensen [12]. Wu used the self-consistent method to derive solutions of the effective bulk modulus and shear modulus for composite materials in which needle-shaped or disk-shaped fillers are oriented randomly [13]. Nguyen derived the effective bulk modulus and shear modulus of three-phase composites containing two types of cylindrical fillers that are randomly oriented two-dimensionally, by using the Mori–Tanaka method, differential scheme, and fast Fourier transformation method [14]. Based on micromechanical analysis using the Eshelby’s equivalent inclusion method [15] and the Mori–Tanaka method, Tandon and Weng obtained the effective elastic moduli of a composite material in which the spheroidal fillers were oriented randomly in two or three-dimensions [16]. However, these analyses are limited to cases where the shape of the fillers is symmetrical such as fibers, spheroids, and disk shapes, and cannot deal with more complex ones such as flakes having major semiaxes of different lengths. Luo and Stevens used the Eshelby’s equivalent inclusion method and the Mori–Tanaka method to derive solutions for effective elastic moduli and thermal expansion coefficient when ellipsoidal fillers were randomly oriented in the material [17,18]. However, their solutions were not in explicit form as they involved coefficients containing the Eshelby’s tensor and inverse matrices. They also derived solutions for the effective elastic moduli in the case of fillers with various shapes and physical properties, but obtained solutions were extremely formal. Similarly, Raju et al. derived solutions of effective elastic moduli by introducing the concept of the differential scheme to the Mori–Tanaka method, but their solutions were also not explicitly expressed [19].

The author’s research group has defined geometrical factors instead of the Eshelby’s tensor to handle continuously the shape of the fillers. By using these factors, we derived the solutions of effective elastic moduli and thermal expansion coefficient for composite materials containing fillers aligned unidirectionally [20]. The obtained solutions were derived in such a way that the terms related to the physical properties of the constituents and the shape of the fillers can be identified. Furthermore, we performed calculations for various shapes of the fillers and clarified that obtained solutions have sufficient accuracy.

In this study, to develop the solutions obtained in our previous research, we examine to formulate explicitly effective elastic moduli and thermal expansion coefficient for composite materials containing ellipsoidal fillers oriented randomly in the material, using the self-consistent method and the Mori–Tanaka method. The analysis based on the self-consistent method differs from that based on the Mori–Tanaka method in the evaluation of the interaction field between fillers. However in these analyses, Eshelby’s equivalent inclusion method is used as a common basic theory, and the same analytical procedure for obtaining the macroscopic stress and strain fields of materials is used. Additionally, we will utilize these solutions to derive effective elastic moduli and thermal expansion coefficient for composite materials and polycrystalline materials where various types of fillers or grains with different shapes and physical properties are oriented randomly in these materials. Using these solutions, we investigate the effects of the shape of the fillers on effective elastic moduli and thermal expansion coefficient. There are several experimental approaches to investigate the effects of filler shapes on the effective elastic properties of composite materials [21–25]. By comparing our analytical results with the upper and lower bounds [6,26] and these experimental results, we will verify the validity and usefulness of our solutions.

## 2. Analysis of effective elastic moduli and thermal expansion coefficient for composite materials containing ellipsoidal fillers oriented randomly

### 2.1. Self-consistent method

#### 2.1.1. Analytical model

**Fig. 1** shows a composite material containing ellipsoidal fillers oriented randomly in the matrix, and the fillers are shown in the shaded area. It is assumed that the fillers and the matrix are completely bonded at their interface. The fillers are classified according to their orientation, and regions of fillers and the whole material are denoted by  $\Omega(i)$  and  $D$  respectively. A global coordinate system  ${}^Gx_i$  is taken along the direction of the stress  ${}^G\sigma_{ij}^0$  acting externally on the material, and a local coordinate system  ${}^{L(i)}x_i$  is taken along the direction of the principal semi-axis of a filler  $\Omega(i)$  as shown in **Fig. 1**. Throughout this study, we will indicate field quantities related to the global or local coordinate system by adding  ${}^G$  or  ${}^{L(i)}$  to the left shoulder of the symbols for field quantities. All fillers have the same ellipsoidal shape, and the axial length of fillers along the direction of  ${}^{L(i)}x_i$  is denoted as  $a_i^\Omega$ . In addition, all fillers are assumed to be isotropic materials with the same physical properties and eigenstrains  $\varepsilon_{ij}^{p\Omega}$ , such as thermal expansion strains. Let  $K^\Omega$ ,  $\mu^\Omega$ , and  $\alpha^\Omega$  represent the bulk modulus, shear modulus, and thermal expansion coefficient of the filler, respectively. While  $K$ ,  $\mu$  and  $\alpha$  represent those of the matrix. Let  $f$  represent the volume fraction of all fillers within the material region  $D$ , and denote the volume fraction of the  $(i)$ th filler as  $f_{(i)}$ . It follows that  $f = \sum_{i=1}^n f_{(i)}$ .

**Fig. 2** shows the model where the material surrounding a filler  $\Omega(i)$ , as shown in **Fig. 1**, is replaced by a material with unknown effective elastic moduli  $\bar{K}$ ,  $\bar{\mu}$  and thermal expansion coefficient  $\bar{\alpha}$ . Note that the overall material exhibits macroscopic isotropy due to the random orientation of the fillers. Furthermore, as shown in **Fig. 3**, we transform the external stress  ${}^G\sigma_{ij}^0$  in **Fig. 2** to  ${}^{L(i)}\sigma_{ij}^0$  in the local coordinate system  ${}^{L(i)}x_i$ . Analysis of the model in **Fig. 2** requires coordinate transformation for the Eshelby’s tensor, which appears in the equivalent equations shown later, so we cannot derive smartly the solutions of the equivalent equation. Therefore, in this analysis, the model in **Fig. 3** will be utilized as the analytical model.

#### 2.1.2. Analysis of effective elastic moduli

In **Fig. 3**, the elastic moduli of the region  $\Omega(i)$  are different from those of the surrounding region  $D - \Omega(i)$ , then the region  $\Omega(i)$  can be treated as a so-called inhomogeneous inclusion. Thus, we consider equivalent equations for replacing the elastic moduli of the filler  $\Omega(i)$  with those of surrounding region  $D - \Omega(i)$  [15]. By resolving stresses and strains into hydrostatic components and deviatoric ones, equivalent equations for each component can be expressed as follows, respectively:

$$\begin{aligned} {}^{L(i)}\sigma_{ii}^0 + {}^{L(i)}\sigma_{ii}^\infty &= 3K^\Omega \left\{ {}^{L(i)}\bar{\epsilon}_{ii} + S_{iikl}^\Omega {}^{L(i)}\epsilon_{kl}^{**\Omega(i)} - \epsilon_{ii}^{p\Omega} \right\} \\ &= 3\bar{K} \left\{ {}^{L(i)}\bar{\epsilon}_{ii} + S_{iikl}^\Omega {}^{L(i)}\epsilon_{kl}^{**\Omega(i)} - {}^{L(i)}\epsilon_{ii}^{**\Omega(i)} \right\}, \end{aligned} \quad (1a)$$

$$\begin{aligned} {}^{L(i)}\sigma_{ij}^0 + {}^{L(i)}\sigma_{ij}^\infty &= 2\mu^\Omega \left\{ {}^{L(i)}\bar{\epsilon}_{ij} + {}'S_{ijkl}^\Omega {}^{L(i)}\epsilon_{kl}^{**\Omega(i)} - {}' \epsilon_{ij}^{p\Omega} \right\} \\ &= 2\bar{\mu} \left\{ {}^{L(i)}\bar{\epsilon}_{ij} + {}'S_{ijkl}^\Omega {}^{L(i)}\epsilon_{kl}^{**\Omega(i)} - {}' \epsilon_{ij}^{p\Omega} \right\}. \end{aligned} \quad (1b)$$

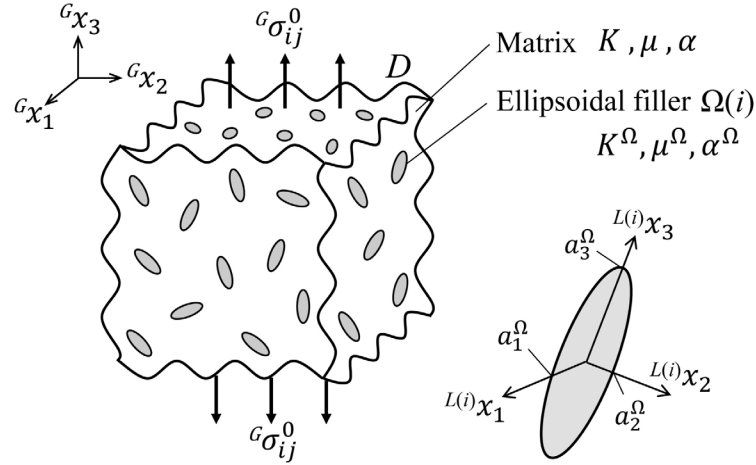


**Fig. 1.** Composite material containing many ellipsoidal fillers oriented randomly.

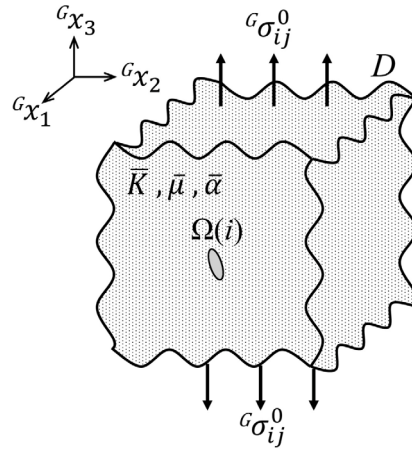


**Fig. 2.** Model smeared out with unknown effective elastic moduli and thermal expansion coefficient in the global coordinate system.

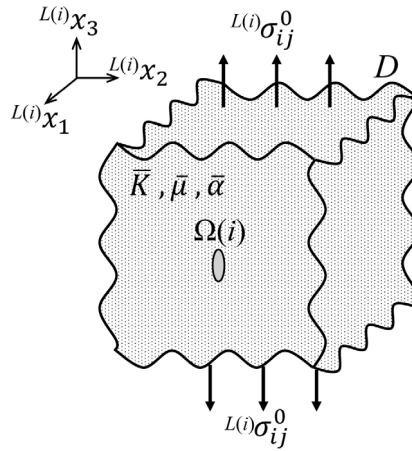


**Fig. 3.** Model smeared out with unknown effective elastic moduli and thermal expansion coefficient in the local coordinate system.

The superscript ' on the left shoulder of the stresses and strains in Eq. (1b) represents the deviatoric component.  $S_{ijkl}^\Omega$  is the Eshelby's tensor in  $\Omega$ , and ' $S_{ijkl}^\Omega$ ' represents the deviatoric component of the Eshelby's tensor, which is given by

$$'S_{ijkl}^\Omega = S_{ijkl}^\Omega - \frac{1}{3}S_{iilk}^\Omega. \quad (2)$$

Excluding the superscript ' on the left shoulder of stresses and strains in Eq. (1b), this equation simultaneously expresses the equivalent expression for shear components.  $L^{(i)}\sigma_{ij}^\infty$  is the eigenstress in  $\Omega(i)$  representing the disturbance of internal stresses.  $L^{(i)}\epsilon_{ij}^{**\Omega(i)}$  is the sum of eigenstrains  $\epsilon_{ij}^{p\Omega}$  and

unknown equivalent eigenstrains  $L^{(i)}\epsilon_{ij}^{*\Omega(i)}$  that substitute for the difference in elastic moduli between the filler and the matrix, and is given by

$$L^{(i)}\epsilon_{ij}^{**\Omega(i)} = \epsilon_{ij}^{p\Omega} + L^{(i)}\epsilon_{ij}^{*\Omega(i)}. \quad (3)$$

$\epsilon_{ij}^{p\Omega}$  in Eq. (3) is given as thermal expansion strains and residual strains in  $\Omega(i)$ . Therefore, since it is obvious that  $\epsilon_{ij}^{p\Omega}$  is a quantity in the local coordinate system,  $L^{(i)}$  indicating that it is a quantity in the local coordinate system is not added to the left shoulder of  $\epsilon_{ij}^{p\Omega}$ . The quantity to be obtained is the equivalent eigenstrain  $L^{(i)}\epsilon_{ij}^{*\Omega(i)}$ . But, to simplify the analysis, we let  $L^{(i)}\epsilon_{ij}^{*\Omega(i)}$  in Eq. (3) be an unknown quantity to be obtained.  $L^{(i)}\bar{\epsilon}_{ij}$  is the strain induced in the whole material by the applied stress  $L^{(i)}\sigma_{ij}^0$ . Araki et al. expressed the Eshelby's tensor  $S_{ijkl}^\Omega$  in a completely separated form into the geometrical factors which include only the aspect ratio of the fillers and the Poisson's ratio of the matrix [20]. Substituting this Eshelby's tensor into the equivalent Eq. (1), and solving for  $L^{(i)}\epsilon_{ij}^{*\Omega(i)}$ , we obtain

$$\begin{aligned} L^{(i)}\epsilon_{11}^{**\Omega(i)} &= -\frac{2(1-\bar{\nu})}{3D_I} \left\langle \left\{ \frac{3}{2}D_{II} + (1+\bar{\nu})G_1 \right\} (L^{(i)}\bar{\epsilon}_{11} - L_K\epsilon_{11}^{p\Omega}) \right. \\ &\quad + \left\{ F_1 + 2(1-2\bar{\nu})G_1 + 2D_{III} \right\} ('L^{(i)}\bar{\epsilon}_{11} - L_\mu'\epsilon_{11}^{p\Omega}) \\ &\quad + \left\{ F_3 - (1-2\bar{\nu})G_3 - D_{III} \right\} ('L^{(i)}\bar{\epsilon}_{22} - L_\mu'\epsilon_{22}^{p\Omega}) \\ &\quad \left. + \left\{ F_2 - (1-2\bar{\nu})G_2 - D_{III} \right\} ('L^{(i)}\bar{\epsilon}_{33} - L_\mu'\epsilon_{33}^{p\Omega}) \right\rangle, \end{aligned} \quad (4a)$$

$$L^{(i)}\epsilon_{23}^{**\Omega(i)} = -\frac{2(1-\bar{\nu})}{D_{IV} + S_1} ('L^{(i)}\bar{\epsilon}_{23} - L_\mu\epsilon_{23}^{p\Omega}). \quad (4b)$$

The other components of strains are obtained by circularly permuting the subscripts of strains 1, 2, and 3. The coefficients in Eq. (4) are summarized in Appendix A.2. The hydrostatic, deviatoric, and shear components of the total strain  $L^{(i)}\epsilon_{ij}^{total}$  in  $\Omega(i)$  in the local coordinate system are given by Eqs. (1)~(4) as follows:

hydrostatic component :

$$\begin{aligned} L^{(i)}\epsilon_{ii}^{total} &= L^{(i)}\bar{\epsilon}_{ii} + S_{iikl}^\Omega L^{(i)}\epsilon_{kl}^{*\Omega(i)}, \\ \therefore L^{(i)}\epsilon_{ii}^{total} &= L^{(i)}\bar{\epsilon}_{ii} - \frac{1}{D_I} \left\langle \left\{ (1+\bar{\nu})D_{II} - 2(1-2\bar{\nu})D_V \right\} (L^{(i)}\bar{\epsilon}_{ii} - L_K\epsilon_{ii}^{p\Omega}) \right. \\ &\quad - \frac{2}{3}(1-2\bar{\nu}) \left[ \left\{ \alpha_1(D_{III} + F_1) - (1+\bar{\nu})G_1 \right\} ('L^{(i)}\bar{\epsilon}_{11} - L_\mu'\epsilon_{11}^{p\Omega}) \right. \\ &\quad + \left\{ \alpha_2(D_{III} + F_2) - (1+\bar{\nu})G_2 \right\} ('L^{(i)}\bar{\epsilon}_{22} - L_\mu'\epsilon_{22}^{p\Omega}) \\ &\quad \left. \left. + \left\{ \alpha_3(D_{III} + F_3) - (1+\bar{\nu})G_3 \right\} ('L^{(i)}\bar{\epsilon}_{33} - L_\mu'\epsilon_{33}^{p\Omega}) \right] \right\rangle, \end{aligned} \quad (5a)$$

deviatoric component :

$$\begin{aligned} 'L^{(i)}\epsilon_{11}^{total} &= 'L^{(i)}\bar{\epsilon}_{11} + \left( S_{11kl}^\Omega - \frac{1}{3}S_{mmkl}^\Omega \right) L^{(i)}\epsilon_{kl}^{*\Omega(i)}, \\ \therefore 'L^{(i)}\epsilon_{11}^{total} &= -('L^{(i)}\bar{\epsilon}_{22} + 'L^{(i)}\bar{\epsilon}_{33}) \\ &\quad - \frac{1}{9D_I} \left\langle 3(1+\bar{\nu}) \left[ \left\{ \frac{2}{3}(1-2\bar{\nu}) + H_1 \right\} G_1 - D_{II}\alpha_1 - \left( 3R_1G_1 - \sum_{i=1}^3 R_iG_i \right) \right] (L^{(i)}\bar{\epsilon}_{ii} - L_K\epsilon_{ii}^{p\Omega}) \right. \\ &\quad + \left[ \left\{ 2(1-2\bar{\nu}) + 3H_1 \right\} (F_2 + 2F_3 - 3D_{III}) + 9 \left\{ R_2F_2 + R_3F_3 + R_2F_3 - D_{III}(R_2 + 2R_3) \right\} \right. \\ &\quad \left. \left. + 2(1+\bar{\nu})(1-2\bar{\nu})(\alpha_2 + \alpha_3)(2G_2 + G_3) \right] ('L^{(i)}\bar{\epsilon}_{22} - L_\mu'\epsilon_{22}^{p\Omega}) \right. \\ &\quad + \left[ \left\{ 2(1-2\bar{\nu}) + 3H_1 \right\} (F_3 + 2F_2 - 3D_{III}) + 9 \left\{ R_2F_2 + R_3F_3 + R_3F_2 - D_{III}(R_3 + 2R_2) \right\} \right. \\ &\quad \left. \left. + 2(1+\bar{\nu})(1-2\bar{\nu})(\alpha_2 + \alpha_3)(2G_3 + G_2) \right] ('L^{(i)}\bar{\epsilon}_{33} - L_\mu'\epsilon_{33}^{p\Omega}) \right\rangle, \end{aligned} \quad (5b)$$

shear component :

$$\begin{aligned} L^{(i)}\epsilon_{23}^{total} &= L^{(i)}\bar{\epsilon}_{23} + 2S_{2323}^\Omega L^{(i)}\epsilon_{23}^{*\Omega(i)}, \\ \therefore L^{(i)}\epsilon_{23}^{total} &= L^{(i)}\bar{\epsilon}_{23} - \frac{1}{D_{IV} + S_1} \left\{ \frac{2}{3}(1-2\bar{\nu}) + H_1 + S_1 \right\} ('L^{(i)}\bar{\epsilon}_{23} - L_\mu\epsilon_{23}^{p\Omega}). \end{aligned} \quad (5c)$$

Other components of  $L^{(i)}\epsilon_{ij}^{total}$  are obtained by circularly permuting the subscripts. The total stress  $L^{(i)}\sigma_{ij}^{total}$  in the region  $\Omega(i)$  in the local coordinate system is given by Eqs. (1) and (5) as follows:

$$\text{hydrostatic component : } L^{(i)}\sigma_{ii}^{total} = L^{(i)}\sigma_{ii}^0 + L^{(i)}\sigma_{ii}^\infty = 3K^\Omega (L^{(i)}\epsilon_{ii}^{total} - \epsilon_{ii}^{p\Omega}), \quad (6a)$$

$$\text{deviatoric component : } 'L^{(i)}\sigma_{ij}^{total} = 'L^{(i)}\sigma_{ij}^0 + 'L^{(i)}\sigma_{ij}^\infty = 2\mu^\Omega ('L^{(i)}\epsilon_{ij}^{total} - \epsilon_{ij}^{p\Omega}), \quad (6b)$$

$$\text{shear component : } L^{(i)}\sigma_{23}^{total} = L^{(i)}\sigma_{23}^0 + L^{(i)}\sigma_{23}^\infty = 2\mu^\Omega (L^{(i)}\epsilon_{23}^{total} - \epsilon_{23}^{p\Omega}). \quad (6c)$$

Eqs. (5) and (6) can be expressed in matrix form as follows:

$$L^{(i)}\epsilon^{total} = \mathbf{P}^\Omega L^{(i)}\bar{\epsilon} - \mathbf{P}^{p\Omega}\epsilon^{p\Omega}, \quad (5d)$$

$$L^{(i)}\sigma^{total} = \mathbf{Q}^\Omega L^{(i)}\bar{\epsilon} - \mathbf{Q}^{p\Omega}\epsilon^{p\Omega}, \quad (6d)$$

where  ${}^{L(i)}\boldsymbol{\varepsilon}^{\text{total}}$ ,  ${}^{L(i)}\boldsymbol{\sigma}^{\text{total}}$ , etc. in the above equations are column vectors consisting of hydrostatic, deviatoric, and shear components, unlike the usual notation. For example,  $\boldsymbol{\varepsilon}$  and  $\boldsymbol{\sigma}$  are defined as

$$\boldsymbol{\varepsilon} = \{\varepsilon_{ii}, ' \varepsilon_{11}, ' \varepsilon_{22}, ' \varepsilon_{33}, \varepsilon_{23}, \varepsilon_{31}, \varepsilon_{12}\}^t, \quad (7a)$$

$$\boldsymbol{\sigma} = \{\sigma_{ii}, ' \sigma_{11}, ' \sigma_{22}, ' \sigma_{33}, \sigma_{23}, \sigma_{31}, \sigma_{12}\}^t. \quad (7b)$$

The coefficient matrices  $\mathbf{P}^\Omega$  and  $\mathbf{P}^{p\Omega}$  in Eqs. (5d) and (6d) are square matrices of  $7 \times 7$ . From Eq. (5), these are given by

$$\mathbf{P}^\Omega = \begin{bmatrix} P_{11}^\Omega & P_{12}^\Omega & P_{13}^\Omega & P_{14}^\Omega & 0 & 0 & 0 \\ P_{21}^\Omega & 0 & P_{23}^\Omega & P_{24}^\Omega & 0 & 0 & 0 \\ P_{31}^\Omega & P_{32}^\Omega & 0 & P_{34}^\Omega & 0 & 0 & 0 \\ P_{41}^\Omega & P_{42}^\Omega & P_{43}^\Omega & 0 & 0 & 0 & 0 \\ 0 & 0 & 0 & 0 & P_{55}^\Omega & 0 & 0 \\ 0 & 0 & 0 & 0 & 0 & P_{66}^\Omega & 0 \\ 0 & 0 & 0 & 0 & 0 & 0 & P_{77}^\Omega \end{bmatrix}, \quad \mathbf{P}^{p\Omega} = \begin{bmatrix} P_{11}^{p\Omega} & P_{12}^{p\Omega} & P_{13}^{p\Omega} & P_{14}^{p\Omega} & 0 & 0 & 0 \\ P_{21}^{p\Omega} & 0 & P_{23}^{p\Omega} & P_{24}^{p\Omega} & 0 & 0 & 0 \\ P_{31}^{p\Omega} & P_{32}^{p\Omega} & 0 & P_{34}^{p\Omega} & 0 & 0 & 0 \\ P_{41}^{p\Omega} & P_{42}^{p\Omega} & P_{43}^{p\Omega} & 0 & 0 & 0 & 0 \\ 0 & 0 & 0 & 0 & P_{55}^{p\Omega} & 0 & 0 \\ 0 & 0 & 0 & 0 & 0 & P_{66}^{p\Omega} & 0 \\ 0 & 0 & 0 & 0 & 0 & 0 & P_{77}^{p\Omega} \end{bmatrix}. \quad (8a)$$

The  $\mathbf{Q}^\Omega$  and  $\mathbf{Q}^{p\Omega}$  are also matrices of the same form as  $\mathbf{P}^\Omega$  and  $\mathbf{P}^{p\Omega}$ , and by substituting Eq. (5d) into Eqs. (6a)~(6c) and comparing these with Eq. (6d), we have

$$\mathbf{Q}^\Omega = \begin{bmatrix} 3K^\Omega P_{11}^\Omega & 3K^\Omega P_{12}^\Omega & 3K^\Omega P_{13}^\Omega & 3K^\Omega P_{14}^\Omega & 0 & 0 & 0 \\ 2\mu^\Omega P_{21}^\Omega & 0 & 2\mu^\Omega P_{23}^\Omega & 2\mu^\Omega P_{24}^\Omega & 0 & 0 & 0 \\ 2\mu^\Omega P_{31}^\Omega & 2\mu^\Omega P_{32}^\Omega & 0 & 2\mu^\Omega P_{34}^\Omega & 0 & 0 & 0 \\ 2\mu^\Omega P_{41}^\Omega & 2\mu^\Omega P_{42}^\Omega & 2\mu^\Omega P_{43}^\Omega & 0 & 0 & 0 & 0 \\ 0 & 0 & 0 & 0 & 2\mu^\Omega P_{55}^\Omega & 0 & 0 \\ 0 & 0 & 0 & 0 & 0 & 2\mu^\Omega P_{66}^\Omega & 0 \\ 0 & 0 & 0 & 0 & 0 & 0 & 2\mu^\Omega P_{77}^\Omega \end{bmatrix},$$

$$\mathbf{Q}^{p\Omega} = \begin{bmatrix} 3K^\Omega(P_{11}^{p\Omega}+1) & 3K^\Omega P_{12}^{p\Omega} & 3K^\Omega P_{13}^{p\Omega} & 3K^\Omega P_{14}^{p\Omega} & 0 & 0 & 0 \\ 2\mu^\Omega P_{21}^{p\Omega} & 0 & 2\mu^\Omega(P_{23}^{p\Omega}-1) & 2\mu^\Omega(P_{24}^{p\Omega}-1) & 0 & 0 & 0 \\ 2\mu^\Omega P_{31}^{p\Omega} & 2\mu^\Omega(P_{32}^{p\Omega}-1) & 0 & 2\mu^\Omega(P_{34}^{p\Omega}-1) & 0 & 0 & 0 \\ 2\mu^\Omega P_{41}^{p\Omega} & 2\mu^\Omega(P_{42}^{p\Omega}-1) & 2\mu^\Omega(P_{43}^{p\Omega}-1) & 0 & 0 & 0 & 0 \\ 0 & 0 & 0 & 0 & 2\mu^\Omega(P_{55}^{p\Omega}+1) & 0 & 0 \\ 0 & 0 & 0 & 0 & 0 & 2\mu^\Omega(P_{66}^{p\Omega}+1) & 0 \\ 0 & 0 & 0 & 0 & 0 & 0 & 2\mu^\Omega(P_{77}^{p\Omega}+1) \end{bmatrix}. \quad (8b)$$

Here we do not show all the components of  $\mathbf{P}^\Omega$  and  $\mathbf{P}^{p\Omega}$  in Eq. (8a). By referring to Eq. (5), some components are given by

$$\begin{aligned} P_{11}^\Omega &= 3(1-\bar{v})(L_K - 1)\frac{D_{II}}{D_I}, & P_{12}^\Omega &= \frac{2(1-2\bar{v})}{3D_I}\{\alpha_1(D_{III} + F_1) - (1+\bar{v})G_1\}, \\ P_{13}^\Omega &= \frac{2(1-2\bar{v})}{3D_I}\{\alpha_2(D_{III} + F_2) - (1+\bar{v})G_2\}, & P_{14}^\Omega &= \frac{2(1-2\bar{v})}{3D_I}\{\alpha_3(D_{III} + F_3) - (1+\bar{v})G_3\}, \\ P_{21}^\Omega &= -\frac{(1+\bar{v})}{3D_I}\left[\left\{\frac{2}{3}(1-2\bar{v})+H_1\right\}G_1 - D_{II}\alpha_1 - \left(3R_1G_1 - \sum_{i=1}^3 R_iG_i\right)\right], \\ P_{23}^\Omega &= -1 - \frac{1}{9D_I}\left[\{2(1-2\bar{v})+3H_1\}(F_2+2F_3-3D_{III}) + 9\{R_2F_2+R_3F_3+R_2F_3-D_{III}(R_2+2R_3)\} \right. \\ &\quad \left. + 2(1+\bar{v})(1-2\bar{v})(\alpha_2+\alpha_3)(2G_2+G_3)\right], \\ P_{24}^\Omega &= -1 - \frac{1}{9D_I}\left[\{2(1-2\bar{v})+3H_1\}(F_3+2F_2-3D_{III}) + 9\{R_2F_2+R_3F_3+R_3F_2-D_{III}(R_3+2R_2)\} \right. \\ &\quad \left. + 2(1+\bar{v})(1-2\bar{v})(\alpha_2+\alpha_3)(2G_3+G_2)\right], \\ P_{55}^\Omega &= 1 - \frac{1}{D_{IV} + S_1}\left\{\frac{2}{3}(1-2\bar{v})+H_1 + S_1\right\}, \\ P_{11}^{p\Omega} &= L_K(P_{11}^\Omega - 1), & P_{12}^{p\Omega} &= L_\mu P_{12}^\Omega, & P_{13}^{p\Omega} &= L_\mu P_{13}^\Omega, & P_{14}^{p\Omega} &= L_\mu P_{14}^\Omega, \\ P_{21}^{p\Omega} &= L_K P_{21}^\Omega, & P_{23}^{p\Omega} &= L_\mu(P_{23}^\Omega + 1), & P_{24}^{p\Omega} &= L_\mu(P_{24}^\Omega + 1), & P_{55}^{p\Omega} &= L_\mu(P_{55}^\Omega - 1). \end{aligned} \quad (9)$$

Next, we consider the coordinate transformation equations for strain and stress from the global coordinate system to the local coordinate one, or vice versa. Let  ${}^L\boldsymbol{\varepsilon}$  and  ${}^L\boldsymbol{\sigma}$  denote the strains and stresses in the local coordinate system, and  ${}^G\boldsymbol{\varepsilon}$  and  ${}^G\boldsymbol{\sigma}$  in the global coordinate one. The coordinate transformation equations are given by

$${}^L\boldsymbol{\sigma} = {}^L(\boldsymbol{\varepsilon}) {}^L\boldsymbol{\sigma}, \quad {}^L\boldsymbol{\varepsilon} = {}^L(\boldsymbol{\varepsilon}) {}^L\boldsymbol{\sigma}, \quad (10a)$$

$${}^G\boldsymbol{\sigma} = {}^L(\boldsymbol{\sigma}) {}^L\boldsymbol{\sigma}, \quad {}^G\boldsymbol{\varepsilon} = {}^L(\boldsymbol{\varepsilon}) {}^L\boldsymbol{\sigma}, \quad (10b)$$

where  $\mathbf{I}$  in the equation is the coordinate transformation matrix given by Eq. (A.11) in Appendix A.3, and  $\mathbf{I}^t$  is the transposed matrix of  $\mathbf{I}$ . The stress and strain in Eq. (10) are given by

$$\boldsymbol{\sigma} = \begin{bmatrix} \sigma_{11} & \sigma_{12} & \sigma_{31} \\ \sigma_{22} & \sigma_{23} & \\ sym. & \sigma_{33} \end{bmatrix}, \quad \boldsymbol{\epsilon} = \begin{bmatrix} \epsilon_{11} & \epsilon_{12} & \epsilon_{31} \\ \epsilon_{22} & \epsilon_{23} & \\ sym. & \epsilon_{33} \end{bmatrix}. \quad (11)$$

Replacing Eq. (11) with the column vectors of hydrostatic, deviatoric, and shear components shown in Eq. (7), the coordinate transformation Eq. (10) is expressed as follows:

$${}^L\boldsymbol{\sigma} = \mathbf{L}({}^G\boldsymbol{\sigma}), \quad {}^L\boldsymbol{\epsilon} = \mathbf{L}({}^G\boldsymbol{\epsilon}), \quad (12a)$$

$${}^G\boldsymbol{\sigma} = \hat{\mathbf{L}}({}^L\boldsymbol{\sigma}), \quad {}^G\boldsymbol{\epsilon} = \hat{\mathbf{L}}({}^L\boldsymbol{\epsilon}), \quad (12b)$$

where the newly defined coordinate transformation matrices  $\mathbf{L}$  and  $\hat{\mathbf{L}}$  are shown in Appendix A.3.

Using the relation of Eq. (12), the transformation equations from the local coordinate system to the global coordinate one for  ${}^{L(i)}\boldsymbol{\epsilon}^{total}$  and  ${}^{L(i)}\boldsymbol{\sigma}^{total}$  expressed by Eqs. (5d) and (6d) are as follows:

$${}^G\boldsymbol{\epsilon}^{total} = \hat{\mathbf{L}}(\mathbf{P}^Q)\mathbf{L}{}^G\bar{\boldsymbol{\epsilon}} - \hat{\mathbf{L}}\mathbf{P}^{pQ}\boldsymbol{\epsilon}^{pQ}, \quad (5e)$$

$${}^G\boldsymbol{\sigma}^{total} = \hat{\mathbf{L}}(\mathbf{Q}^Q)\mathbf{L}{}^G\bar{\boldsymbol{\epsilon}} - \hat{\mathbf{L}}\mathbf{Q}^{pQ}\boldsymbol{\epsilon}^{pQ}. \quad (6e)$$

Using the strain and stress in Eqs. (5e) and (6e), the total macroscopic strain  ${}^G\bar{\boldsymbol{\epsilon}}$  and stress  ${}^G\bar{\boldsymbol{\sigma}}$  of the material are obtained as

$$\begin{aligned} {}^G\bar{\boldsymbol{\epsilon}} &= \sum_{i=1}^n f_{(i)} {}^G\boldsymbol{\epsilon}^{total} + \left(1 - \sum_{i=1}^n f_{(i)}\right) {}^G\boldsymbol{\epsilon}^m \\ &= \frac{1}{8\pi^2} f \int_0^\pi \int_0^{2\pi} \int_0^{2\pi} \sin\theta (\hat{\mathbf{L}}(\mathbf{P}^Q)\mathbf{L}{}^G\bar{\boldsymbol{\epsilon}} - \hat{\mathbf{L}}\mathbf{P}^{pQ}\boldsymbol{\epsilon}^{pQ}) d\theta d\phi d\psi + (1-f) {}^G\boldsymbol{\epsilon}^m \\ &= f(\mathbf{P}^\Sigma {}^G\bar{\boldsymbol{\epsilon}} - \mathbf{P}^{p\Sigma} \boldsymbol{\epsilon}^{pQ}) + (1-f) {}^G\boldsymbol{\epsilon}^m, \end{aligned} \quad (13a)$$

$$\begin{aligned} {}^G\bar{\boldsymbol{\sigma}} &= \sum_{i=1}^n f_{(i)} {}^G\boldsymbol{\sigma}^{total} + \left(1 - \sum_{i=1}^n f_{(i)}\right) {}^G\boldsymbol{\sigma}^m \\ &= \frac{1}{8\pi^2} f \int_0^\pi \int_0^{2\pi} \int_0^{2\pi} \sin\theta (\hat{\mathbf{L}}(\mathbf{Q}^Q)\mathbf{L}{}^G\bar{\boldsymbol{\epsilon}} - \hat{\mathbf{L}}\mathbf{Q}^{pQ}\boldsymbol{\epsilon}^{pQ}) d\theta d\phi d\psi + (1-f) {}^G\boldsymbol{\sigma}^m \\ &= f(\mathbf{Q}^\Sigma {}^G\bar{\boldsymbol{\epsilon}} - \mathbf{Q}^{p\Sigma} \boldsymbol{\epsilon}^{pQ}) + (1-f) {}^G\boldsymbol{\sigma}^m. \end{aligned} \quad (14a)$$

Eq. (A.12) in Appendix A.3 is used to derive the above equations.  ${}^G\boldsymbol{\epsilon}^m$  in Eq. (13a) and  ${}^G\boldsymbol{\sigma}^m$  in Eq. (14a) are the total strain and stress in the matrix, and are given as a column vector with the same component arrangement as in Eq. (7).  $\mathbf{P}^\Sigma$ ,  $\mathbf{P}^{p\Sigma}$ ,  $\mathbf{Q}^\Sigma$  and  $\mathbf{Q}^{p\Sigma}$  are given in the simple form as

$$\mathbf{X}^\Sigma = \begin{bmatrix} X_h^\Sigma & 0 & 0 & 0 & 0 & 0 & 0 \\ 0 & X_d^\Sigma & 0 & 0 & 0 & 0 & 0 \\ 0 & 0 & X_d^\Sigma & 0 & 0 & 0 & 0 \\ 0 & 0 & 0 & X_d^\Sigma & 0 & 0 & 0 \\ 0 & 0 & 0 & 0 & X_d^\Sigma & 0 & 0 \\ 0 & 0 & 0 & 0 & 0 & X_d^\Sigma & 0 \\ 0 & 0 & 0 & 0 & 0 & 0 & X_d^\Sigma \end{bmatrix}, \quad \mathbf{X}^{p\Sigma} = \begin{bmatrix} X_h^{p\Sigma} & X_1^{p\Sigma} & X_2^{p\Sigma} & X_3^{p\Sigma} & 0 & 0 & 0 \\ 0 & 0 & 0 & 0 & 0 & 0 & 0 \\ 0 & 0 & 0 & 0 & 0 & 0 & 0 \\ 0 & 0 & 0 & 0 & 0 & 0 & 0 \\ 0 & 0 & 0 & 0 & 0 & 0 & 0 \\ 0 & 0 & 0 & 0 & 0 & 0 & 0 \\ 0 & 0 & 0 & 0 & 0 & 0 & 0 \end{bmatrix}, \quad (X = P, Q). \quad (15)$$

In particular, for  $\mathbf{P}^\Sigma$  and  $\mathbf{Q}^\Sigma$ , only the diagonal terms are present and the off-diagonal terms are all zero. Furthermore, we can see that the number of independent components of  $\mathbf{P}^\Sigma$  and  $\mathbf{Q}^\Sigma$  is two, similar to the elastic moduli of isotropic materials.  $P_h^\Sigma$ ,  $P_d^\Sigma$ ,  $P_h^{p\Sigma}$ ,  $P_i^{p\Sigma}$ , etc. in Eq. (15) are given by

$$P_h^\Sigma = 3(1-\bar{v})(L_K - 1) \frac{D_{II}}{D_I}, \quad P_d^\Sigma = \frac{2}{5}(1-\bar{v})(L_\mu - 1) \left( \frac{2D_{III}}{D_I} + D^\Sigma \right), \quad (16)$$

$$P_h^{p\Sigma} = L_K \left\{ 3(1-\bar{v})(L_K - 1) \frac{D_{II}}{D_I} - 1 \right\}, \quad P_i^{p\Sigma} = \frac{2(1-2\bar{v})L_\mu}{3D_I} \{ \alpha_i(D_{III} + F_i) - (1+\bar{v})G_i \}, \quad (16)$$

$$Q_h^\Sigma = 3K^\Omega P_h^\Sigma, \quad Q_d^\Sigma = 2\mu^\Omega P_d^\Sigma, \quad (17)$$

$$Q_h^{p\Sigma} = 3K^\Omega (P_h^{p\Sigma} + 1), \quad Q_i^{p\Sigma} = 3K^\Omega P_i^{p\Sigma}. \quad (17)$$

As can be seen from Eqs. (13) to (15), we find that deviatoric components of  ${}^G\bar{\boldsymbol{\epsilon}}$  and  ${}^G\bar{\boldsymbol{\sigma}}$  are the same as shear ones of them. Therefore, Eq. (13a) and Eq. (14a) can be separated into the hydrostatic component and the deviatoric one, and can be expressed as follows:

$${}^G\bar{\epsilon}_{ii} = f(P_h^\Sigma {}^G\bar{\epsilon}_{ii} - P_h^{p\Sigma} \boldsymbol{\epsilon}_{ii}^{pQ} - P_1^{p\Sigma} {}' \boldsymbol{\epsilon}_{11}^{pQ} - P_2^{p\Sigma} {}' \boldsymbol{\epsilon}_{22}^{pQ} - P_3^{p\Sigma} {}' \boldsymbol{\epsilon}_{33}^{pQ}) + (1-f) {}^G\boldsymbol{\epsilon}_{ii}^m, \quad (13b)$$

$${}^G\bar{\epsilon}_{ij} = f P_d^\Sigma {}' G\bar{\epsilon}_{ij} + (1-f) {}' G\boldsymbol{\epsilon}_{ij}^m, \quad (13c)$$

$${}^G\bar{\sigma}_{ii} = 3f K^\Omega \{ P_h^\Sigma {}^G\bar{\epsilon}_{ii} - (P_h^{p\Sigma} + 1) \boldsymbol{\epsilon}_{ii}^{pQ} - P_1^{p\Sigma} {}' \boldsymbol{\epsilon}_{11}^{pQ} - P_2^{p\Sigma} {}' \boldsymbol{\epsilon}_{22}^{pQ} - P_3^{p\Sigma} {}' \boldsymbol{\epsilon}_{33}^{pQ} \} + (1-f) {}^G\boldsymbol{\sigma}_{ii}^m, \quad (14b)$$

$${}^G\bar{\sigma}_{ij} = 2f \mu^\Omega P_d^\Sigma {}' G\bar{\epsilon}_{ij} + (1-f) {}' G\boldsymbol{\sigma}_{ij}^m. \quad (14c)$$

The relation between shear stresses and strains is obtained by removing the superscript ' from Eqs. (13c) and (14c). The following relations hold between  $\boldsymbol{\epsilon}_{ij}^m$  and  $\boldsymbol{\sigma}_{ij}^m$  in the matrix:

$$G\boldsymbol{\sigma}_{ii}^m = 3K {}^G\boldsymbol{\epsilon}_{ii}^m, \quad , \quad {}' G\boldsymbol{\sigma}_{ij}^m = 2\mu {}' G\boldsymbol{\epsilon}_{ij}^m, \quad (18)$$

where  $K$  and  $\mu$  are bulk modulus and shear modulus of the matrix respectively, as shown in Fig. 1. For Eqs. (13b)~(14c), by eliminating  $\epsilon_{ij}^m$  and  $\sigma_{ij}^m$  using the relation of Eq. (18), we obtain the relation between  ${}^G\bar{\epsilon}_{ij}$  and  ${}^G\bar{\sigma}_{ij}$  as follows:

$$\begin{aligned} {}^G\bar{\sigma}_{ii} &= 3\{K + f(K^\Omega - K)P_h^\Sigma\} {}^G\bar{\epsilon}_{ii} - 3fK^\Omega \epsilon_{ii}^{p\Omega} \\ &\quad - 3f(K^\Omega - K)(P_h^{p\Sigma} \epsilon_{ii}^{p\Omega} + P_1^{p\Sigma} \epsilon_{11}^{p\Omega} + P_2^{p\Sigma} \epsilon_{22}^{p\Omega} + P_3^{p\Sigma} \epsilon_{33}^{p\Omega}), \end{aligned} \quad (19a)$$

$${}^G\bar{\sigma}_{ij} = 2\{\mu + f(\mu^\Omega - \mu)P_d^\Sigma\} {}^G\bar{\epsilon}_{ij}. \quad (19b)$$

If the eigenstrain  $\epsilon_{ij}^{p\Omega}$  is zero, the total strain  ${}^G\bar{\epsilon}_{ij}$  is equal to the elastic strain. Then, the relations between  ${}^G\bar{\epsilon}_{ij}$  and  ${}^G\bar{\sigma}_{ij}$  by using the effective bulk modulus  $\bar{K}$  and shear modulus  $\bar{\mu}$  are given as follows:

$${}^G\bar{\sigma}_{ii} = 3\bar{K} {}^G\bar{\epsilon}_{ii}, \quad {}^G\bar{\sigma}_{ij} = 2\bar{\mu} {}^G\bar{\epsilon}_{ij}. \quad (20)$$

After substituting  $\epsilon_{ij}^{p\Omega} = 0$  into Eq. (19), we set Eq. (19) equal to Eq. (20). Substituting  $P_h^\Sigma$  and  $P_d^\Sigma$  in Eq. (16) and  $L_K$  and  $L_\mu$  in Eq. (A.5) into equated expressions, we finally obtain the effective bulk modulus  $\bar{K}$  and shear modulus  $\bar{\mu}$  as follows:

$$\bar{K} = K + f(K^\Omega - K)P_h^\Sigma = K + 3f(1 - \bar{v}) \bar{K} \left( \frac{K^\Omega - K}{K^\Omega - \bar{K}} \right) \frac{D_{II}}{D_I}, \quad (21a)$$

$$\bar{\mu} = \mu + f(\mu^\Omega - \mu)P_d^\Sigma = \mu + \frac{2}{5}f(1 - \bar{v}) \bar{\mu} \left( \frac{\mu^\Omega - \mu}{\mu^\Omega - \bar{\mu}} \right) \left( \frac{2D_{III}}{D_I} + D^\Sigma \right), \quad (21b)$$

where  $\bar{v}$  is the effective Poisson's ratio of the material. As shown in Appendix A.2,  $D_I$ ,  $D_{II}$ ,  $D_{III}$  and  $D^\Sigma$  in Eq. (21) contain the unknown effective elastic moduli  $\bar{K}$ ,  $\bar{\mu}$  and  $\bar{v}$ . Therefore, Eq. (21) represents an equation for determining these unknown moduli. Since the physical properties of the material are isotropic, the following relation holds among  $\bar{\mu}$ ,  $\bar{K}$  and  $\bar{v}$ :

$$\bar{v} = \frac{3\bar{K} - 2\bar{\mu}}{6\bar{K} + 2\bar{\mu}}. \quad (22)$$

Substituting Eq. (22) into Eq. (21) gives equations for the unknown  $\bar{K}$  and  $\bar{\mu}$ .

If the shape of the fillers is spherical, substituting the geometrical factors in Appendix A.1 into the coefficients in Appendix A.2, we obtain  $\alpha_i = 0$ ,  $\beta_i = 2/15$ ,  $R_i = F_i = G_i = S_i = 0$ . Therefore,  $D_I$  to  $D_{III}$  and  $D^\Sigma$  in Eq. (A.3) in Appendix A.2 are as follows:

$$D_I = L_I D_{IV}^2, \quad D_{II} = D_{IV}^2, \quad D_{III} = L_I D_{IV}, \quad D^\Sigma = \frac{3}{D_{IV}}. \quad (23)$$

Substituting Eqs. (23), (A.3) and (A.5) in Appendix A.2 into Eq. (21), we obtain

$$\bar{K} = K + \frac{3f(1 - \bar{v}) \bar{K} (K^\Omega - K)}{3(1 - \bar{v})\bar{K} + (1 + \bar{v})(K^\Omega - \bar{K})}, \quad \bar{\mu} = \mu + \frac{15f(1 - \bar{v}) \bar{\mu} (\mu^\Omega - \mu)}{15(1 - \bar{v})\bar{\mu} + 2(4 - 5\bar{v})(\mu^\Omega - \bar{\mu})}. \quad (24)$$

These solutions completely agree with those derived by Budiansky [10].

### 2.1.3. Analysis of effective thermal expansion coefficient

For the model shown in Fig. 3, consider the state where the external stress  ${}^G\sigma_{ij}^0 = 0$  and only the temperature change  $\Delta T$  occurs in the material. Then, thermal expansion strains occur in the material due to the difference in the thermal expansion coefficient between the filler and the matrix. When the thermal expansion of the homogenized material surrounding the filler  $\Omega(i)$  is regarded as the reference, the thermal expansion strain  $\epsilon_{ij}^{p\Omega}$  occurred in  $\Omega(i)$  is expressed by

$$\epsilon_{ij}^{p\Omega} = \delta_{ij}(\alpha^\Omega - \bar{\alpha})\Delta T, \quad (25)$$

where  $\alpha^\Omega$  is the thermal expansion coefficient of the filler, and  $\bar{\alpha}$  is the unknown effective thermal expansion coefficient of the homogenized material as shown in Fig. 3.

The hydrostatic components of the total strain and stress of the filler  $\Omega(i)$  are obtained from Eqs. (5d), (6d), and (25) as follows:

$${}^{L(i)}\epsilon_{ii}^{total} = -3P_{11}^{p\Omega}(\alpha^\Omega - \bar{\alpha})\Delta T + 3\bar{\alpha}\Delta T, \quad (26a)$$

$${}^{L(i)}\sigma_{ii}^{total} = -9K^\Omega(P_{11}^{p\Omega} + 1)(\alpha^\Omega - \bar{\alpha})\Delta T, \quad (27a)$$

where we note that the thermal expansion strain  $3\bar{\alpha}\Delta T$  must be added to the total strain  ${}^{L(i)}\epsilon_{ii}^{total}$ , since  ${}^{L(i)}\epsilon_{ii}^{total}$  is solved by referring the thermal expansion of the homogenized material. Transforming Eqs. (26a) and (27a) to the global coordinate system and taking the sum of the total strain and stress in fillers and the matrix, the hydrostatic components of the macroscopic total strain and stress of the material are given by the following equations, respectively:

$${}^G\bar{\epsilon}_{ii} = -3fP_h^\Sigma(\alpha^\Omega - \bar{\alpha})\Delta T + 3f\bar{\alpha}\Delta T + (1 - f){}^G\epsilon_{ii}^m = 3\bar{\alpha}\Delta T, \quad (26b)$$

$${}^G\bar{\sigma}_{ii} = -9fK^\Omega(P_h^{p\Sigma} + 1)(\alpha^\Omega - \bar{\alpha})\Delta T + (1 - f){}^G\sigma_{ii}^m = 0, \quad (27b)$$

where  ${}^G\bar{\epsilon}_{ii}$  is the thermal expansion strain of the whole material itself, so  ${}^G\bar{\epsilon}_{ii}$  is  $3\bar{\alpha}\Delta T$  as shown on the right side of Eq. (26b). In addition,  ${}^G\bar{\sigma}_{ii}$  in Eq. (27b) is the sum of the internal stresses in the material, so  ${}^G\bar{\sigma}_{ii}$  must be zero. Solving Eq. (27b) for the total stress  ${}^G\sigma_{ii}^m$  in the matrix yields

$${}^G\sigma_{ii}^m = \frac{9f}{1-f}K^\Omega(P_h^{p\Sigma} + 1)(\alpha^\Omega - \bar{\alpha})\Delta T. \quad (28)$$

The total strain  ${}^G\epsilon_{ij}^m$  of the matrix is given by the sum of the elastic strain  ${}^G\epsilon_{ij}^{me}$  and the thermal expansion strain  $3\alpha\Delta T$  of the matrix. Therefore, the hydrostatic component of  ${}^G\epsilon_{ij}^m$  is obtained from Eqs. (18) and (28) as follows:

$${}^G\epsilon_{ii}^m = {}^G\epsilon_{ii}^{me} + 3\alpha\Delta T = \frac{G\sigma_{ii}^m}{3K} + 3\alpha\Delta T = \frac{3f}{1-f} \frac{K^\Omega}{K} (P_h^{p\Sigma} + 1)(\alpha^\Omega - \bar{\alpha})\Delta T + 3\alpha\Delta T . \quad (29)$$

Substituting Eqs. (29) and (16) into Eq. (26b) and using the relation in Eq. (21a), the effective thermal expansion coefficient  $\bar{\alpha}$  finally becomes to be

$$\begin{aligned} \bar{\alpha} &= \alpha + \frac{f\{(K^\Omega - K)P_h^{p\Sigma} + K^\Omega\}(\alpha^\Omega - \alpha)}{(1-f)K + f\{(K^\Omega - K)P_h^{p\Sigma} + K^\Omega\}} = \alpha + 3f(1-\bar{\nu}) \frac{K^\Omega}{K^\Omega - K} \frac{D_{II}}{D_I} (\alpha^\Omega - \alpha) \\ &= \alpha + \frac{K^\Omega(\bar{K} - K)}{\bar{K}(K^\Omega - K)} (\alpha^\Omega - \alpha) . \end{aligned} \quad (30)$$

The last expression of Eq. (30) is derived from the fact that the third expression of Eq. (30) and  $\bar{K}$  of Eq. (21) consist of the same coefficients. This relation shows that  $\bar{\alpha}$  and  $\bar{K}$  are closely related from the viewpoint of the volume change of the material. From this meaning, it can be said that Eqs. (21) and (30) are physically consistent solutions. Furthermore, based on the last expression of Eq. (30), if we determine the effective bulk modulus  $\bar{K}$  in Eq. (21),  $\bar{\alpha}$  can be automatically determined as well.

When the shape of the fillers is spherical, by substituting Eq. (23) into Eq. (30),  $\bar{\alpha}$  reduces to

$$\bar{\alpha} = \alpha + \frac{3f(1-\bar{\nu})K^\Omega(\alpha^\Omega - \alpha)}{3(1-\bar{\nu})\bar{K} + (1+\bar{\nu})(K^\Omega - \bar{K})} . \quad (31)$$

## 2.2. Mori–tanaka method

In this section, we derive effective elastic moduli and effective thermal expansion coefficient of composite materials based on the Mori–Tanaka method. In this theory, the interaction due to the existence of many fillers is represented by unknown interaction stresses  $\tilde{\sigma}_{ij}$ , which act on the whole material. That is, the region surrounding the filler  $\Omega(i)$  in Fig. 3 is smeared out by unknown interaction stresses  $\tilde{\sigma}_{ij}$  instead of unknown elastic moduli  $\bar{K}$ ,  $\bar{\mu}$ , and the thermal expansion coefficient  $\bar{\alpha}$ . Therefore, the elastic moduli and thermal expansion coefficient in this region are  $K$ ,  $\mu$ , and  $\alpha$  of the matrix, respectively. The strains corresponding to the external stress  $\sigma_{ij}^0$  and the interaction stress  $\tilde{\sigma}_{ij}$  are represented by  $\epsilon_{ij}^0$  and  $\tilde{\epsilon}_{ij}$ , respectively. Then, the equivalent equations of the filler  $\Omega(i)$  is expressed as follows by referring to Eq. (1)

$$\begin{aligned} {}^{L(i)}\sigma_{ii}^0 + {}^{L(i)}\tilde{\sigma}_{ii} + {}^{L(i)}\sigma_{ii}^\infty &= 3K^\Omega \left\{ {}^{L(i)}\epsilon_{ii}^0 + {}^{L(i)}\tilde{\epsilon}_{ii} + S_{ijkl}^{\Omega} {}^{L(i)}\epsilon_{kl}^{**\Omega(i)} - \epsilon_{ii}^{p\Omega} \right\} \\ &= 3K \left\{ {}^{L(i)}\epsilon_{ii}^0 + {}^{L(i)}\tilde{\epsilon}_{ii} + S_{ijkl}^{\Omega} {}^{L(i)}\epsilon_{kl}^{**\Omega(i)} - {}^{L(i)}\epsilon_{ii}^{**\Omega(i)} \right\} , \end{aligned} \quad (32a)$$

$$\begin{aligned} {}'^{L(i)}\sigma_{ij}^0 + {}'^{L(i)}\tilde{\sigma}_{ij} + {}'^{L(i)}\sigma_{ij}^\infty &= 2\mu^\Omega \left\{ {}'^{L(i)}\epsilon_{ij}^0 + {}'^{L(i)}\tilde{\epsilon}_{ij} + {}'S_{ijkl}^{\Omega} {}^{L(i)}\epsilon_{kl}^{**\Omega(i)} - {}' \epsilon_{ij}^{p\Omega} \right\} \\ &= 2\mu \left\{ {}'^{L(i)}\epsilon_{ij}^0 + {}'^{L(i)}\tilde{\epsilon}_{ij} + {}'S_{ijkl}^{\Omega} {}^{L(i)}\epsilon_{kl}^{**\Omega(i)} - {}'^{L(i)}\epsilon_{ij}^{**\Omega(i)} \right\} , \end{aligned} \quad (32b)$$

where the following relations hold between  $\sigma_{ij}^0$  and  $\epsilon_{ij}^0$ ,  $\tilde{\sigma}_{ij}$  and  $\tilde{\epsilon}_{ij}$ , respectively.

$$\sigma_{ii}^0 = 3K\epsilon_{ii}^0 , \quad {}'\sigma_{ij}^0 = 2\mu {}' \epsilon_{ij}^0 , \quad (33a)$$

$$\tilde{\sigma}_{ii} = 3K\tilde{\epsilon}_{ii} , \quad {}'\tilde{\sigma}_{ij} = 2\mu {}' \tilde{\epsilon}_{ij} . \quad (33b)$$

Comparing Eqs. (1) and (32), we can see that Eq. (32) is a simple replacement of Eq. (1) as follows:

$$\begin{aligned} \sigma_{ij}^0 &\rightarrow \sigma_{ij}^0 + \tilde{\sigma}_{ij} , \quad \tilde{\epsilon}_{ij} \rightarrow \epsilon_{ij}^0 + \tilde{\epsilon}_{ij} , \\ \bar{K} &\rightarrow K , \quad \bar{\mu} \rightarrow \mu , \quad \bar{\nu} \rightarrow \nu . \end{aligned} \quad (34)$$

Therefore, the subsequent calculations are performed by replacing the equations in Section 2.1 with Eq. (34), so the coefficients that appear in the equations have the same form as those used in Section 2.1. However, it should be noted that the unknown effective elastic moduli  $\bar{K}$ ,  $\bar{\mu}$  and  $\bar{\nu}$  appearing in Eqs. (9), (16) and (17) are replaced by the known elastic moduli of the matrix  $K$ ,  $\mu$  and  $\nu$ .

From the above, the macroscopic total strain  ${}^G\epsilon_{ij}$  and stress  ${}^G\tilde{\sigma}_{ij}$  are as follows by referring to Eqs. (13) and (14)

$$\begin{aligned} {}^G\tilde{\epsilon}_{ii} &= f \left\{ P_h^\Sigma ({}^G\epsilon_{ii}^0 + {}^G\tilde{\epsilon}_{ii}) - P_h^{p\Sigma} \epsilon_{ii}^{p\Omega} - P_1^{p\Sigma} {}'\epsilon_{11}^{p\Omega} - P_2^{p\Sigma} {}'\epsilon_{22}^{p\Omega} - P_3^{p\Sigma} {}'\epsilon_{33}^{p\Omega} \right\} + (1-f) {}^G\sigma_{ii}^m \\ &= \{fP_h^\Sigma + (1-f)\} ({}^G\epsilon_{ii}^0 + {}^G\tilde{\epsilon}_{ii}) - f(P_h^{p\Sigma} \epsilon_{ii}^{p\Omega} + P_1^{p\Sigma} {}'\epsilon_{11}^{p\Omega} + P_2^{p\Sigma} {}'\epsilon_{22}^{p\Omega} + P_3^{p\Sigma} {}'\epsilon_{33}^{p\Omega}) , \end{aligned} \quad (35b)$$

$${}'^G\tilde{\epsilon}_{ij} = f P_d^\Sigma ({}'^G\epsilon_{ij}^0 + {}'^G\tilde{\epsilon}_{ij}) + (1-f) {}'^G\sigma_{ij}^m = \{fP_d^\Sigma + (1-f)\} ({}'^G\epsilon_{ij}^0 + {}'^G\tilde{\epsilon}_{ij}) , \quad (35c)$$

$$\begin{aligned} {}^G\tilde{\sigma}_{ii} &= 3fK^\Omega \left\{ P_h^\Sigma ({}^G\epsilon_{ii}^0 + {}^G\tilde{\epsilon}_{ii}) - (P_h^{p\Sigma} + 1)\epsilon_{ii}^{p\Omega} - P_1^{p\Sigma} {}'\epsilon_{11}^{p\Omega} - P_2^{p\Sigma} {}'\epsilon_{22}^{p\Omega} - P_3^{p\Sigma} {}'\epsilon_{33}^{p\Omega} \right\} + (1-f) {}^G\sigma_{ii}^m \\ &= 3\{fK^\Omega P_h^\Sigma + (1-f)K\} ({}^G\epsilon_{ii}^0 + {}^G\tilde{\epsilon}_{ii}) - 3fK^\Omega \left\{ (P_h^{p\Sigma} + 1)\epsilon_{ii}^{p\Omega} + P_1^{p\Sigma} {}'\epsilon_{11}^{p\Omega} + P_2^{p\Sigma} {}'\epsilon_{22}^{p\Omega} + P_3^{p\Sigma} {}'\epsilon_{33}^{p\Omega} \right\} , \end{aligned} \quad (36b)$$

$${}'^G\tilde{\sigma}_{ij} = 2f\mu^\Omega P_d^\Sigma ({}'^G\epsilon_{ij}^0 + {}'^G\tilde{\epsilon}_{ij}) + (1-f) {}'^G\sigma_{ij}^m = 2\{f\mu^\Omega P_d^\Sigma + (1-f)\mu\} ({}'^G\epsilon_{ij}^0 + {}'^G\tilde{\epsilon}_{ij}) , \quad (36c)$$

where  ${}^G\epsilon_{ij}^m$  and  ${}^G\sigma_{ij}^m$  are the total strain and stress of the matrix, and given by the sum of the external fields and interaction ones. Between  ${}^G\epsilon_{ij}^m$  and  ${}^G\sigma_{ij}^m$ , the same relation as Eq. (18) holds. That is,

$$\begin{aligned} {}^G\epsilon_{ij}^m &= {}^G\epsilon_{ij}^0 + {}^G\tilde{\epsilon}_{ij} , \quad {}^G\sigma_{ij}^m = {}^G\sigma_{ij}^0 + {}^G\tilde{\sigma}_{ij} , \\ {}^G\sigma_{ii}^m &= 3K {}^G\epsilon_{ii}^m , \quad {}'^G\sigma_{ij}^m = 2\mu {}'^G\epsilon_{ij}^m . \end{aligned} \quad (37)$$

These relations are used in the derivation of the last expression in Eqs. (35) and (36).

In Eqs. (35) and (36), by substituting  $\epsilon_{ij}^{p\Omega} = 0$  and eliminating  $({}^G\epsilon_{ij}^0 + {}^G\tilde{\epsilon}_{ij}^0)$ , we can find the relation between  ${}^G\bar{\epsilon}_{ij}$  and  ${}^G\bar{\sigma}_{ij}$ . Equating the obtained relation with Eq. (20), the effective bulk modulus  $\bar{K}$  and shear modulus  $\bar{\mu}$  are given by

$$\bar{K} = K + \frac{3f(1-\nu)K \frac{D_{II}}{D_I}}{(1-f) + 3f(1-\nu) \frac{K}{K^\Omega - K} \frac{D_{II}}{D_I}}, \quad \bar{\mu} = \mu + \frac{\frac{2}{5}f(1-\nu)\mu \left( \frac{2D_{III}}{D_I} + D^\Sigma \right)}{(1-f) + \frac{2}{5}f(1-\nu) \frac{\mu}{\mu^\Omega - \mu} \left( \frac{2D_{III}}{D_I} + D^\Sigma \right)}, \quad (38)$$

where  $D_I$ ,  $D_{II}$ ,  $D_{III}$  and  $D^\Sigma$  have the same form as shown in [Appendix A.2](#). However, as previously mentioned, we note that the unknown elastic moduli  $K$ ,  $\mu$  and  $\nu$  included in these coefficients are replaced by the known elastic moduli of the matrix  $K$ ,  $\mu$ , and  $\nu$ .

From this derivation process, it is interesting that the Mori-Tanaka method can give directly explicit solutions of effective elastic moduli without obtaining unknown interaction fields  $\tilde{\sigma}_{ij}$  and  $\tilde{\epsilon}_{ij}$ . The interaction stress  $\tilde{\sigma}_{ij}$  can be obtained from the condition that the total internal stress in the whole material is zero. Since  ${}^G\bar{\sigma}_{ij}$  in Eqs. (35) and (36) is given by the sum of the external stress  ${}^G\sigma_{ij}^0$  and the total internal stress, subtracting the stress  ${}^G\sigma_{ij}^0$  from  ${}^G\bar{\sigma}_{ij}$  yields zero. Therefore, from Eqs. (35), (36), and (33), the interaction strain  $\tilde{\epsilon}_{ij}$  can be obtained as

$$\begin{aligned} {}^G\bar{\sigma}_{ij} - {}^G\sigma_{ij}^0 &= 0, \\ \therefore {}^G\tilde{\epsilon}_{ii} &= \frac{f \left( 1 - \frac{K^\Omega}{K} P_h^\Sigma \right) {}^G\epsilon_{ii}^0 + \frac{K^\Omega}{K} \left\{ (P_h^{p\Sigma} + 1) \epsilon_{ii}^{p\Omega} + P_1^{p\Sigma} \epsilon_{11}^{p\Omega} + P_2^{p\Sigma} \epsilon_{22}^{p\Omega} + P_3^{p\Sigma} \epsilon_{33}^{p\Omega} \right\}}{1 - f \left( 1 - \frac{K^\Omega}{K} P_h^\Sigma \right)}, \end{aligned} \quad (39)$$

$$\therefore {}^G\tilde{\epsilon}_{ij} = \frac{f \left( 1 - \frac{\mu^\Omega}{\mu} P_d^\Sigma \right)}{1 - f \left( 1 - \frac{\mu^\Omega}{\mu} P_d^\Sigma \right)} {}^G\epsilon_{ij}^0. \quad (40)$$

The interaction stress  $\tilde{\sigma}_{ij}$  is obtained by substituting Eqs. (39) and (40) into Eq. (33b).

Next, we derive the effective thermal expansion coefficient  $\bar{\alpha}$  of the material. Similar to the previous section, we consider the state where only the temperature change  $\Delta T$  is applied, with the external stress  $\sigma_{ij}^0 = 0$ . Therefore, we substitute  $\epsilon_{ij}^0 = 0$  into Eqs. (35) and (36). In the same way as Eq. (25), the thermal expansion strain that occurs in the filler  $\Omega(i)$  when the thermal expansion of the matrix is regarded as the reference can be expressed by

$$\epsilon_{ij}^{p\Omega} = \delta_{ij}(\alpha^\Omega - \alpha)\Delta T. \quad (41)$$

From this equation, the hydrostatic components in Eqs. (35) and (36) are as follows:

$${}^G\bar{\epsilon}_{ii} = \left\{ f P_h^\Sigma + (1-f) \right\} {}^G\tilde{\epsilon}_{ii} - 3f P_h^{p\Sigma} (\alpha^\Omega - \alpha) \Delta T + 3\alpha \Delta T = 3\bar{\alpha} \Delta T, \quad (42b)$$

$${}^G\bar{\sigma}_{ii} = 3 \left\{ f K^\Omega P_h^\Sigma + (1-f)K \right\} {}^G\tilde{\epsilon}_{ii} - 9f K^\Omega (P_h^{p\Sigma} + 1)(\alpha^\Omega - \alpha) \Delta T = 0, \quad (43b)$$

where we note that  $3\alpha \Delta T$  is added to the total strain  ${}^G\bar{\epsilon}_{ii}$  because of the same reason as the derivation of Eq. (26b).

Similar to Eq. (26b),  ${}^G\bar{\epsilon}_{ii}$  is the thermal expansion strain of the whole material, that is  $3\bar{\alpha} \Delta T$ . Eq. (43b) is the sum of the internal stresses in the material and becomes to be zero. Solving this equation for the interaction strain  ${}^G\tilde{\epsilon}_{ii}$  yields

$${}^G\tilde{\epsilon}_{ii} = \frac{3f K^\Omega (P_h^{p\Sigma} + 1)}{f K^\Omega P_h^\Sigma + (1-f)K} (\alpha^\Omega - \alpha) \Delta T. \quad (44)$$

Substituting Eqs. (44) and (16) into Eq. (42b) and solving for the effective thermal expansion coefficient  $\bar{\alpha}$  yields

$$\bar{\alpha} = \alpha + \frac{3f(1-\nu) \left( \frac{K^\Omega}{K^\Omega - K} \right) \frac{D_{II}}{D_I} (\alpha^\Omega - \alpha)}{(1-f) + 3f(1-\nu) \left( \frac{K^\Omega}{K^\Omega - K} \right) \frac{D_{II}}{D_I}} = \alpha + \frac{K^\Omega (\bar{K} - K)}{K(K^\Omega - K)} (\alpha^\Omega - \alpha). \quad (45)$$

The last expression of Eq. (45) is derived from the fact that the second expression of Eq. (45) and  $\bar{K}$  of Eq. (38) are composed of the same coefficients. This relation is interesting because it is the same as Eq. (30). From this relation,  $\bar{\alpha}$  can be calculated from  $\bar{K}$ .

In the case where the shape of the fillers is spherical, the same relation as Eq. (23) holds, so Eqs. (38) and (45) are reduced to

$$\bar{K} = K + \frac{3f(1-\nu)K(K^\Omega - K)}{3(1-\nu)K + (1-f)(1+\nu)(K^\Omega - K)}, \quad \bar{\mu} = \mu + \frac{15f(1-\nu)\mu(\mu^\Omega - \mu)}{15(1-\nu)\mu + 2(1-f)(4-5\nu)(\mu^\Omega - \mu)}, \quad (46)$$

$$\bar{\alpha} = \alpha + \frac{3f(1-\nu)K^\Omega(\alpha^\Omega - \alpha)}{3(1-\nu)K^\Omega - 2(1-f)(1-2\nu)(K^\Omega - K)}. \quad (47)$$

These solutions completely agree with those obtained by Kanaun and Levin [27]. Comparing Eqs. (46) and (47) with Eqs. (24) and (31) obtained by the self-consistent method, it is also interesting that these equations are very similar.

### 3. Analysis of effective elastic moduli and thermal expansion coefficient for composite materials (or polycrystalline materials) containing various types of fillers (or crystal grains)

#### 3.1. Analytical model

[Fig. 4](#) shows a composite material in which various types of ellipsoidal fillers (or crystal grains) with different physical properties and shapes are oriented randomly in the material. Similar to the model in [Fig. 1](#), it is assumed that the fillers and the matrix are completely bonded at their

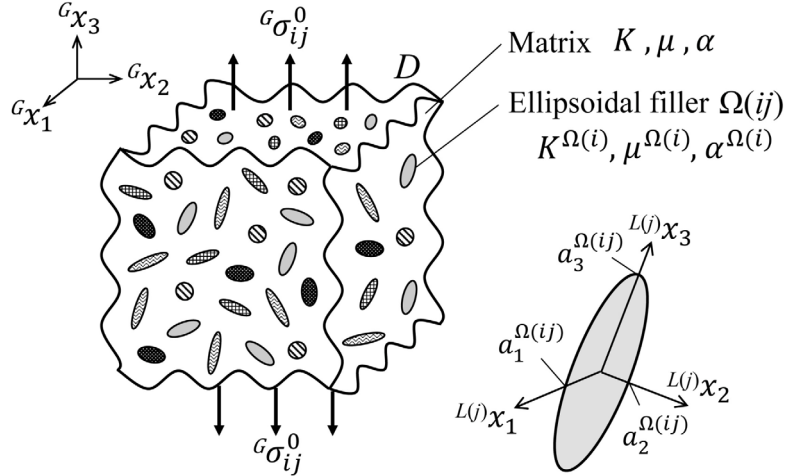


**Fig. 4.** Composite material containing many ellipsoidal fillers with different physical properties and shapes oriented randomly. (If there is no matrix, this model becomes a polycrystalline material.)

interface. The fillers are classified by  $(i)$  in terms of their physical properties and shapes. Therefore, as shown in Fig. 4, we add the superscript  $(i)$  to the right shoulder of the elastic moduli and thermal expansion coefficient of the filler, and assume that there are  $n$  kinds of fillers. Although not shown in the figure, the eigenstrain is similarly classified by  $(i)$  and expressed by  $\varepsilon_{ij}^{p\Omega(i)}$ . The orientation is classified by  $(j)$ , and it is assumed that there are  $m$  types of orientation. Since all fillers are oriented randomly, there are  $m$  types of orientations for every  $(i)$ th filler. Let  $\Omega(ij)$  denote the region of the filler with physical properties and shape  $(i)$  and orientation  $(j)$ , and  $f_{(ij)}$  denote the volume fraction of  $\Omega(ij)$ . The total volume fraction of the fillers, denoted by  $f$ , is calculated as  $f = \sum_{i=1}^n \sum_{j=1}^m f_{(ij)}$ . If there is no matrix, the model in Fig. 4 corresponds to polycrystalline materials.

### 3.2. Self-consistent method

As shown in Section 2, the region surrounding a filler  $\Omega(ij)$  is smeared out with a material with unknown effective elastic moduli  $\bar{K}$ ,  $\bar{\mu}$  and thermal expansion coefficient  $\bar{\alpha}$ . Solving the equivalent equation in the local coordinate system  $L(j)x_i$  taken along the direction of the principal semi-axis of  $\Omega(ij)$  and referring to Eqs. (5d) and (6d), the total strain and stress of  $\Omega(ij)$  can be obtained as follows:

$$L(j)\boldsymbol{\varepsilon}^{total} = \mathbf{P}^{\Omega(i)} L(j)\bar{\boldsymbol{\varepsilon}} - \mathbf{P}^{p\Omega(i)} \boldsymbol{\varepsilon}^{p\Omega(i)}, \quad (48d)$$

$$L(j)\boldsymbol{\sigma}^{total} = \mathbf{Q}^{\Omega(i)} L(j)\bar{\boldsymbol{\sigma}} - \mathbf{Q}^{p\Omega(i)} \boldsymbol{\varepsilon}^{p\Omega(i)}, \quad (49d)$$

where  $\mathbf{P}^{\Omega(i)}$ ,  $\mathbf{P}^{p\Omega(i)}$ ,  $\mathbf{Q}^{\Omega(i)}$  and  $\mathbf{Q}^{p\Omega(i)}$  have the same matrix form as Eq. (8), and their components have the same form as Eq. (9). However, it should be noted that the coefficients related to the shape and physical properties of the fillers in Eq. (9) are represented by  $D_1^{(i)} \sim D_V^{(i)}$ ,  $F_i^{(i)}$ ,  $G_i^{(i)}$ ,  $a_i^{(i)}$ ,  $R_i^{(i)}$  and  $L_K^{(i)}$  classified by  $(i)$ .

Referring to Eqs. (5e) and (6e), the transforming Eqs. (48d) and (49d) to the global coordinate system yields following equations

$$G\boldsymbol{\varepsilon}^{total} = \hat{\mathbf{L}}^{(j)}(\mathbf{P}^{\Omega(i)} \mathbf{L}^{(j)} G\bar{\boldsymbol{\varepsilon}} - \hat{\mathbf{L}}^{(j)} \mathbf{P}^{p\Omega(i)} \boldsymbol{\varepsilon}^{p\Omega(i)}), \quad (48e)$$

$$G\boldsymbol{\sigma}^{total} = \hat{\mathbf{L}}^{(j)}(\mathbf{Q}^{\Omega(i)} \mathbf{L}^{(j)} G\bar{\boldsymbol{\sigma}} - \hat{\mathbf{L}}^{(j)} \mathbf{Q}^{p\Omega(i)} \boldsymbol{\varepsilon}^{p\Omega(i)}). \quad (49e)$$

Using the total strains and stresses in Eqs. (48e) and (49e) and referring to Eqs. (13) and (14), the total macroscopic strain  $G\bar{\boldsymbol{\varepsilon}}$  and stress  $G\bar{\boldsymbol{\sigma}}$  of the material are obtained as

$$\begin{aligned} G\bar{\boldsymbol{\varepsilon}} &= \sum_{i=1}^n \sum_{j=1}^m f_{(ij)} G\boldsymbol{\varepsilon}^{total} + \left(1 - \sum_{i=1}^n \sum_{j=1}^m f_{(ij)}\right) G\boldsymbol{\varepsilon}^m \\ &= \sum_{i=1}^n \frac{f_{(i)}}{8\pi^2} \int_0^\pi \int_0^{2\pi} \int_0^{2\pi} \sin\theta \left( \hat{\mathbf{L}}(\mathbf{P}^{\Omega(i)}) \mathbf{L} G\bar{\boldsymbol{\varepsilon}} - \hat{\mathbf{L}} \mathbf{P}^{p\Omega(i)} \boldsymbol{\varepsilon}^{p\Omega(i)} \right) d\theta d\phi d\psi + (1-f) G\boldsymbol{\varepsilon}^m \\ &= \sum_{i=1}^n f_{(i)} (\mathbf{P}^{\Sigma(i)} G\bar{\boldsymbol{\varepsilon}} - \mathbf{P}^{p\Sigma(i)} \boldsymbol{\varepsilon}^{p\Omega(i)}) + (1-f) G\boldsymbol{\varepsilon}^m, \end{aligned} \quad (50a)$$

$$\begin{aligned} G\bar{\boldsymbol{\sigma}} &= \sum_{i=1}^n \sum_{j=1}^m f_{(ij)} G\boldsymbol{\sigma}^{total} + \left(1 - \sum_{i=1}^n \sum_{j=1}^m f_{(ij)}\right) G\boldsymbol{\sigma}^m \\ &= \sum_{i=1}^n \frac{f_{(i)}}{8\pi^2} \int_0^\pi \int_0^{2\pi} \int_0^{2\pi} \sin\theta \left( \hat{\mathbf{L}}(\mathbf{Q}^{\Omega(i)}) \mathbf{L} G\bar{\boldsymbol{\sigma}} - \hat{\mathbf{L}} \mathbf{Q}^{p\Omega(i)} \boldsymbol{\varepsilon}^{p\Omega(i)} \right) d\theta d\phi d\psi + (1-f) G\boldsymbol{\sigma}^m \\ &= \sum_{i=1}^n f_{(i)} (\mathbf{Q}^{\Sigma(i)} G\bar{\boldsymbol{\sigma}} - \mathbf{Q}^{p\Sigma(i)} \boldsymbol{\varepsilon}^{p\Omega(i)}) + (1-f) G\boldsymbol{\sigma}^m. \end{aligned} \quad (51a)$$

$\mathbf{P}^{\Sigma(i)}$ ,  $\mathbf{P}^{p\Sigma(i)}$ ,  $\mathbf{Q}^{\Sigma(i)}$  and  $\mathbf{Q}^{p\Sigma(i)}$  have the same matrix form as Eq. (15), and their components have the same form as Eqs. (16) and (17).

Similar to Eqs. (13) and (14), Eqs. (50a) and (51a) can be expressed as equations for the hydrostatic component and the deviatoric one as follows:

$${}^G\bar{\epsilon}_{ii} = \sum_{i=1}^n f_{(i)} \left\{ P_h^{\Sigma(i)} {}^G\bar{\epsilon}_{ii} - P_h^{p\Sigma(i)} \epsilon_{ii}^{p\Omega(i)} - P_1^{p\Sigma(i)}' \epsilon_{11}^{p\Omega(i)} - P_2^{p\Sigma(i)}' \epsilon_{22}^{p\Omega(i)} - P_3^{p\Sigma(i)}' \epsilon_{33}^{p\Omega(i)} \right\} + (1-f) {}^G\epsilon_{ii}^m, \quad (50b)$$

$${}'^G\bar{\epsilon}_{ij} = \sum_{i=1}^n f_{(i)} P_d^{\Sigma(i)} {}'^G\bar{\epsilon}_{ij} + (1-f) {}'^G\epsilon_{ij}^m, \quad (50c)$$

$${}^G\bar{\sigma}_{ii} = 3 \sum_{i=1}^n f_{(i)} K^{\Omega(i)} \left\{ P_h^{\Sigma(i)} {}^G\bar{\epsilon}_{ii} - (P_h^{p\Sigma(i)} + 1) \epsilon_{ii}^{p\Omega(i)} - P_1^{p\Sigma(i)}' \epsilon_{11}^{p\Omega(i)} - P_2^{p\Sigma(i)}' \epsilon_{22}^{p\Omega(i)} - P_3^{p\Sigma(i)}' \epsilon_{33}^{p\Omega(i)} \right\} + (1-f) {}^G\sigma_{ii}^m, \quad (51b)$$

$${}'^G\bar{\sigma}_{ij} = 2 \sum_{i=1}^n f_{(i)} \mu^{\Omega(i)} P_d^{\Sigma(i)} {}'^G\bar{\epsilon}_{ij} + (1-f) {}'^G\sigma_{ij}^m. \quad (51c)$$

The relation between shear stresses and strains is obtained by removing subscript ' $'$  from Eqs. (50c) and (51c). From Eqs. (50), (51), and (18), the relation between  ${}^G\bar{\epsilon}_{ij}$  and  ${}^G\bar{\sigma}_{ij}$  can be obtained. Substituting  $\epsilon_{ij}^{p\Omega(i)} = 0$  in this relation and equating it with Eq. (20), the effective bulk modulus  $\bar{K}$  and the shear modulus  $\bar{\mu}$  are finally obtained as

$$\bar{K} = K + \sum_{i=1}^n f_{(i)} (K^{\Omega(i)} - K) P_h^{\Sigma(i)} = K + 3(1 - \bar{\nu}) \bar{K} \sum_{i=1}^n f_{(i)} \left( \frac{K^{\Omega(i)} - K}{K^{\Omega(i)} - \bar{K}} \right) \frac{D_{II}^{(i)}}{D_I^{(i)}}, \quad (52a)$$

$$\bar{\mu} = \mu + \sum_{i=1}^n f_{(i)} (\mu^{\Omega(i)} - \mu) P_d^{\Sigma(i)} = \mu + \frac{2(1 - \bar{\nu})}{5} \bar{\mu} \sum_{i=1}^n f_{(i)} \left( \frac{\mu^{\Omega(i)} - \mu}{\mu^{\Omega(i)} - \bar{\mu}} \right) \left( \frac{2D_{III}^{(i)}}{D_I^{(i)}} + D^{\Sigma(i)} \right). \quad (52b)$$

When the shape of the fillers is spherical, by substituting the relation shown in Eq. (23) into Eq. (52),  $\bar{K}$  and  $\bar{\mu}$  reduce to

$$\bar{K} = K + 3(1 - \bar{\nu}) \bar{K} \sum_{i=1}^n f_{(i)} \frac{K^{\Omega(i)} - K}{3(1 - \bar{\nu}) \bar{K} + (1 + \bar{\nu})(K^{\Omega(i)} - \bar{K})}, \quad (53a)$$

$$\bar{\mu} = \mu + 15(1 - \bar{\nu}) \bar{\mu} \sum_{i=1}^n f_{(i)} \frac{\mu^{\Omega(i)} - \mu}{15(1 - \bar{\nu}) \bar{\mu} + 2(4 - 5\bar{\nu})(\mu^{\Omega(i)} - \bar{\mu})}. \quad (53b)$$

These solutions agree with those obtained by Li and Wang [28].

In the case of polycrystalline materials, since there is no matrix, i.e.,  $f = 1$  in Eqs. (50) and (51),  $\bar{K}$  and  $\bar{\mu}$  can be obtained as

$$\bar{K} = 3(1 - \bar{\nu}) \bar{K} \sum_{i=1}^n f_{(i)} \left( \frac{K^{\Omega(i)} - K}{K^{\Omega(i)} - \bar{K}} \right) \frac{D_{II}^{(i)}}{D_I^{(i)}}, \quad \bar{\mu} = \frac{2(1 - \bar{\nu})}{5} \bar{\mu} \sum_{i=1}^n f_{(i)} \left( \frac{\mu^{\Omega(i)} - \mu}{\mu^{\Omega(i)} - \bar{\mu}} \right) \left( \frac{2D_{III}^{(i)}}{D_I^{(i)}} + D^{\Sigma(i)} \right). \quad (54)$$

In Eq. (54), if there is only one type of filler, i.e.,  $n = 1$ , we obtain the following relation by substituting the coefficients in Appendix A.2 into  $\bar{K}$  in Eq. (54):

$$2(1 - 2\bar{\nu})(K^{\Omega} - \bar{K})D_V(D_{II} + 1) = 0.$$

A nontrivial solution that satisfies this equation is  $\bar{K} = K^{\Omega}$ . Substituting this into  $\bar{\mu}$  in Eq. (54) yields

$$1 - \frac{2(1 - \bar{\nu})\mu^{\Omega}}{5} \left[ \frac{2 \left\{ 2(1 - \bar{\nu})\mu^{\Omega} + (H_I - 1 - \frac{1-2\bar{\nu}}{3})(\mu^{\Omega} - \bar{\mu}) \right\}}{\left\{ 2(1 - \bar{\nu})\mu^{\Omega} + (H_I - 1 - \frac{1-2\bar{\nu}}{3})(\mu^{\Omega} - \bar{\mu}) \right\}^2 - \frac{3}{2} \sum_{i=1}^3 R_i^2 (\mu^{\Omega} - \bar{\mu})^2} + \sum_{i=1}^3 \frac{1}{2(1 - \bar{\nu})\mu^{\Omega} + (H_I - 1 - \frac{1-2\bar{\nu}}{3} + S_i)(\mu^{\Omega} - \bar{\mu})} \right] = 0.$$

$\bar{\mu}$  that satisfies the above equation is immediately found to be  $\mu^{\Omega}$ . From the above, it can be seen that the solution of Eq. (54) is a physically consistent solution in the limiting case of  $f = 1$ .

Next, the effective thermal expansion coefficient of the material is considered. As shown in Section 2.1.3, we consider the state where the external stress  $\sigma_{ij}^0 = 0$  and only the temperature change  $\Delta T$  occurs. When the thermal expansion of the homogenized material surrounding the fillers is regarded as the reference, the thermal expansion strain occurred in the fillers is given by,

$$\epsilon_{ij}^{p\Omega(i)} = \delta_{ij}(\alpha^{\Omega(i)} - \bar{\alpha})\Delta T, \quad (55)$$

where  $\alpha^{\Omega(i)}$  is the coefficient of thermal expansion of the filler  $\Omega(ij)$ . The hydrostatic components of the total strain and stress of the filler  $\Omega(ij)$  are given as follows by referring to Eqs. (26a) and (27a)

$${}^{L(j)}\epsilon_{ii}^{total} = -3P_{11}^{p\Omega(i)}(\alpha^{\Omega(i)} - \bar{\alpha})\Delta T + 3\bar{\alpha}\Delta T, \quad (56a)$$

$${}^{L(j)}\sigma_{ii}^{total} = -9K^{\Omega(i)}(P_{11}^{p\Omega(i)} + 1)(\alpha^{\Omega(i)} - \bar{\alpha})\Delta T. \quad (57a)$$

Transforming Eqs. (56a) and (57a) to the global coordinate system and taking the sum of the total strain and stress in fillers and the matrix, the hydrostatic components of the macroscopic total strain and stress of the material are given as follows by referring to Eqs. (26b) and (27b)

$${}^G\bar{\epsilon}_{ii} = -3 \sum_{i=1}^n f_{(i)} P_h^{p\Sigma(i)} (\alpha^{\Omega(i)} - \bar{\alpha})\Delta T + 3f\bar{\alpha}\Delta T + (1-f) {}^G\epsilon_{ii}^m = 3\bar{\alpha}\Delta T, \quad (56b)$$

$${}^G\bar{\sigma}_{ii} = -9 \sum_{i=1}^n f_{(i)} K^{\Omega(i)} (P_h^{p\Sigma(i)} + 1)(\alpha^{\Omega(i)} - \bar{\alpha})\Delta T + (1-f) {}^G\sigma_{ii}^m = 0. \quad (57b)$$

We can obtain the total stress  ${}^G\sigma_{ii}^m$  in the matrix from Eq. (57b), and derive the total strain  ${}^G\varepsilon_{ii}^m$  in the matrix, similar to Eqs. (28) and (29). Substituting obtained  ${}^G\varepsilon_{ii}^m$  into Eq. (56b) and solving for the effective thermal expansion coefficient, we have

$$\bar{\alpha} = \alpha + \frac{\sum_{i=1}^n f_{(i)} \{ (K^{\Omega(i)} - K) P_h^{p\Sigma(i)} + K^{\Omega(i)} \} (\alpha^{\Omega(i)} - \alpha)}{(1-f)K + \sum_{i=1}^n f_{(i)} \{ (K^{\Omega(i)} - K) P_h^{p\Sigma(i)} + K^{\Omega(i)} \}}. \quad (58)$$

In the case of polycrystalline materials, there is no matrix, so  $\bar{\alpha}$  reduces to

$$\bar{\alpha} = \frac{\sum_{i=1}^n f_{(i)} K^{\Omega(i)} (1 + P_h^{p\Sigma(i)}) \alpha^{\Omega(i)}}{\sum_{i=1}^n f_{(i)} K^{\Omega(i)} (1 + P_h^{p\Sigma(i)})}. \quad (59)$$

In Eq. (59), when the type of filler is only one ( $n = 1$ ), it is easy to find that  $\bar{\alpha} = \alpha^\Omega$ . Therefore, Eq. (59) is also a physically consistent solution.

### 3.3. Mori–tanaka method

Similar to Section 2.2, the solution of effective elastic moduli can be obtained by replacing the solutions obtained in the previous section with Eqs. (34) and (37). Therefore, from Eqs. (50) and (51), the total macroscopic strain  ${}^G\bar{\varepsilon}$  and stress  ${}^G\bar{\sigma}$  of the material are given as follows:

$$\begin{aligned} {}^G\bar{\varepsilon}_{ii} &= \left\{ \sum_{i=1}^n f_{(i)} P_h^{\Sigma(i)} + (1-f) \right\} ({}^G\varepsilon_{ii}^0 + {}^G\tilde{\varepsilon}_{ii}) \\ &\quad - \sum_{i=1}^n f_{(i)} \left\{ P_h^{p\Sigma(i)} \varepsilon_{ii}^{p\Omega(i)} + P_1^{p\Sigma(i)}' \varepsilon_{11}^{p\Omega(i)} + P_2^{p\Sigma(i)}' \varepsilon_{22}^{p\Omega(i)} + P_3^{p\Sigma(i)}' \varepsilon_{33}^{p\Omega(i)} \right\}, \end{aligned} \quad (60b)$$

$${}^G\bar{\varepsilon}_{ij} = \left\{ \sum_{i=1}^n f_{(i)} P_d^{\Sigma(i)} + (1-f) \right\} ({}^G\varepsilon_{ij}^0 + {}^G\tilde{\varepsilon}_{ij}), \quad (60c)$$

$$\begin{aligned} {}^G\bar{\sigma}_{ii} &= 3 \left\{ \sum_{i=1}^n f_{(i)} K^{\Omega(i)} P_h^{\Sigma(i)} + (1-f)K \right\} ({}^G\varepsilon_{ii}^0 + {}^G\tilde{\varepsilon}_{ii}) \\ &\quad - 3 \sum_{i=1}^n f_{(i)} K^{\Omega(i)} \left\{ (P_h^{p\Sigma(i)} + 1) \varepsilon_{ii}^{p\Omega(i)} + P_1^{p\Sigma(i)}' \varepsilon_{11}^{p\Omega(i)} + P_2^{p\Sigma(i)}' \varepsilon_{22}^{p\Omega(i)} + P_3^{p\Sigma(i)}' \varepsilon_{33}^{p\Omega(i)} \right\}, \end{aligned} \quad (61b)$$

$${}^G\bar{\sigma}_{ij} = 2 \left\{ \sum_{i=1}^n f_{(i)} \mu^{\Omega(i)} P_d^{\Sigma(i)} + (1-f)\mu \right\} ({}^G\varepsilon_{ij}^0 + {}^G\tilde{\varepsilon}_{ij}). \quad (61c)$$

Substituting  $\varepsilon_{ij}^{p\Omega(i)} = 0$  and eliminating  $({}^G\varepsilon_{ij}^0 + {}^G\tilde{\varepsilon}_{ij})$  in Eqs. (60) and (61), we can find the relation between  ${}^G\bar{\varepsilon}_{ij}$  and  ${}^G\bar{\sigma}_{ij}$ . Equating the obtained relation with Eq. (20), the effective bulk modulus  $\bar{K}$  and shear modulus  $\bar{\mu}$  are given by

$$\bar{K} = K + \frac{3(1-\nu)K \sum_{i=1}^n f_{(i)} \frac{D_{II}^{(i)}}{D_1^{(i)}}}{(1-f) + 3(1-\nu)K \sum_{i=1}^n f_{(i)} \frac{1}{K^{\Omega(i)} - K} \frac{D_{II}^{(i)}}{D_1^{(i)}}}, \quad (62a)$$

$$\bar{\mu} = \mu + \frac{\frac{2}{5}(1-\nu)\mu \sum_{i=1}^n f_{(i)} \left( \frac{2D_{III}^{(i)}}{D_1^{(i)}} + D^{\Sigma(i)} \right)}{(1-f) + \frac{2}{5}(1-\nu)\mu \sum_{i=1}^n f_{(i)} \frac{1}{\mu^{\Omega(i)} - \mu} \left( \frac{2D_{III}^{(i)}}{D_1^{(i)}} + D^{\Sigma(i)} \right)}. \quad (62b)$$

Next, we consider the effective thermal expansion coefficient of the material. As shown in the previous section, we consider the state where the external stress  $\sigma_{ij}^0 = 0$  and only the temperature change  $\Delta T$  occurs. In the same way as Eq. (41), the thermal expansion strain that occurs in the filler  $\Omega(ij)$  when the thermal expansion of the matrix is regarded as the reference is expressed by

$$\varepsilon_{ij}^{p\Omega(i)} = \delta_{ij}(\alpha^{\Omega(i)} - \alpha)\Delta T. \quad (63)$$

From the above, the hydrostatic components in Eqs. (60) and (61) are given by

$${}^G\bar{\varepsilon}_{ii} = \left\{ \sum_{i=1}^n f_{(i)} P_h^{\Sigma(i)} + (1-f) \right\} {}^G\tilde{\varepsilon}_{ii} - 3 \sum_{i=1}^n f_{(i)} P_h^{p\Sigma(i)} (\alpha^{\Omega(i)} - \alpha) \Delta T + 3\alpha \Delta T = 3\bar{\alpha} \Delta T, \quad (64b)$$

$${}^G\bar{\sigma}_{ii} = 3 \left\{ \sum_{i=1}^n f_{(i)} K^{\Omega(i)} P_h^{\Sigma(i)} + (1-f)K \right\} {}^G\tilde{\varepsilon}_{ii} - 9 \sum_{i=1}^n f_{(i)} K^{\Omega(i)} (P_h^{p\Sigma(i)} + 1) (\alpha^{\Omega(i)} - \alpha) \Delta T = 0. \quad (65b)$$

The interaction strain  ${}^G\tilde{\varepsilon}_{ii}$  can be obtained from Eq. (65b). Substituting this  ${}^G\tilde{\varepsilon}_{ii}$  into Eq. (64b), the effective thermal expansion coefficient  $\bar{\alpha}$  is obtained as

$$\bar{\alpha} = \alpha - \sum_{i=1}^n f_{(i)} P_h^{p\Sigma(i)} (\alpha^{\Omega(i)} - \alpha) + \frac{\left\{ \sum_{i=1}^n f_{(i)} P_h^{\Sigma(i)} + (1-f) \right\} \sum_{i=1}^n f_{(i)} K^{\Omega(i)} (P_h^{p\Sigma(i)} + 1) (\alpha^{\Omega(i)} - \alpha)}{\left\{ \sum_{i=1}^n f_{(i)} K^{\Omega(i)} P_h^{\Sigma(i)} + (1-f)K \right\}}. \quad (66)$$

**Table 1**

Elastic constants and thermal expansion coefficient of constituents used in the experiment of Takahashi et al.

Constituents	Young's modulus (GPa)	Poisson's ratio	Thermal expansion coefficient $\times 10^{-6}$ (1/K)
Matrix (epoxy)	2.3	0.41	50
Filler (glass)	69.1	0.22	5

**Table 2**

Elastic constants and thermal expansion coefficient of constituents used in the experiment of Okuno.

Constituents	Young's modulus (GPa)	Poisson's ratio
Matrix (polypropylene)	1.47	0.35
Filler (phlogopite mica)	147.10	0.11

**Table 3**

Elastic constants and thermal expansion coefficient of constituents used in the experiment of Miwa et al.

Constituents	Young's modulus (GPa)	Poisson's ratio	Thermal expansion coefficient $\times 10^{-6}$ (1/K)
Matrix (epoxy)	20 °C	1.90	0.30
	40 °C	1.82	0.32
	60 °C	1.63	0.35
Filler (glass)	87.5	0.21	6.6

For polycrystalline materials, substituting  $f = 1$  for Eqs. (62) and (66), and taking the limits  $K \rightarrow 0$ ,  $\mu \rightarrow 0$  and  $\alpha \rightarrow 0$ , we obtain the solutions of effective elastic moduli and thermal expansion coefficient as follows:

$$\bar{K} = \frac{\sum_{i=1}^n f_{(i)} \frac{D_{II}^{(i)}}{D_I^{(i)}}}{\sum_{i=1}^n f_{(i)} \frac{1}{K^{\Omega(i)}} \frac{D_{II}^{(i)}}{D_I^{(i)}}}, \quad \bar{\mu} = \frac{\sum_{i=1}^n f_{(i)} \left( \frac{2D_{III}^{(i)}}{D_I^{(i)}} + D^{\Sigma(i)} \right)}{\sum_{i=1}^n f_{(i)} \frac{1}{\mu^{\Omega(i)}} \left( \frac{2D_{III}^{(i)}}{D_I^{(i)}} + D^{\Sigma(i)} \right)}, \quad (67)$$

$$\bar{\alpha} = - \sum_{i=1}^n f_{(i)} P_h^{\rho\Sigma(i)} \alpha^{\Omega(i)} + \frac{\sum_{i=1}^n f_{(i)} P_h^{\Sigma(i)} \sum_{i=1}^n f_{(i)} K^{\Omega(i)} (P_h^{\rho\Sigma(i)} + 1) \alpha^{\Omega(i)}}{\sum_{i=1}^n f_{(i)} K^{\Omega(i)} P_h^{\Sigma(i)}}. \quad (68)$$

In Eqs. (67) and (68), when the type of filler is only one ( $n = 1$ ), we find that  $\bar{K} = K^\Omega$ ,  $\bar{\mu} = \mu^\Omega$  and  $\bar{\alpha} = \alpha^\Omega$ . Therefore, it can be seen that Eqs. (67) and (68) are physically consistent solutions like Eqs. (54) and (59) obtained by the self-consistent method.

#### 4. Numerical calculations and discussions

##### 4.1. Physical properties of constituents used in calculations

In this chapter, we utilize the solutions obtained in Chapters 2 and 3 to calculate the effective elastic moduli and thermal expansion coefficient of composites containing ellipsoidal fillers oriented randomly. The upper and lower bounds of these physical properties for two-phase composites have been solved by Hashin and Shtrikman [6] and Rosen and Hashin [26]. In these analyses, it is assumed that the shape of each phase is arbitrary and the effective physical properties of the material are isotropic. Using variational principles, they show the range of possible values of effective physical properties from the viewpoint of energy. First, we confirm whether the results of our analysis are within the range of these upper and lower bounds. On the other hand, Takahashi et al. experimentally investigated the effects of the shape and the volume fraction of the glass fillers on the effective Young's modulus for the composite material in which the glass fillers are oriented randomly in the epoxy matrix [21]. Okuno made composite materials containing mica flakes in polypropylene and experimentally evaluated the effect of the aspect ratio of the mica flakes on the effective Young's modulus of the material [22]. In addition, Miwa et al. fabricated composite materials in which short glass fibers contained in epoxy and experimentally clarified the effect of the aspect ratio of the glass fibers on the effective thermal expansion coefficient of the material [23]. In the experiment by Miwa et al. they also considered the temperature dependence of the elastic moduli and thermal expansion coefficient of epoxy resin as shown in Table 3. By comparing our analytical results with these experimental ones, we will verify the usefulness of analytical solutions for actual materials. In calculating effective elastic moduli and thermal expansion coefficient, we assume the composite materials are the same as those used in these experiments, and use elastic constants and thermal expansion coefficient of constituents given in Tables 1 to 3.

##### 4.2. Effective elastic moduli and thermal expansion coefficient

In this section, before comparing the experimental results, we will first discuss whether the effective elastic moduli and thermal expansion coefficients obtained by this analysis can theoretically give consistent and valid results for all shapes of ellipsoidal fillers. In this verification, the material constants in Table 1 are used.

Fig. 5 shows the change in the effective bulk modulus  $\bar{K}$  as the aspect ratio of the fillers is continuously changed for each shape shown in Fig. A.1. In the figure, the solid red line is the result of the self-consistent method (denoted by SC(3D)), and the solid blue line is that of the Mori-Tanaka method (denoted by MT(3D)). The result when the fillers are oriented unidirectionally (denoted by MT (unidirectional)) is also shown by the dotted line. The vertical axis of the figure is  $\bar{K}/K$ , which is dimensionless with the bulk modulus  $K$  of the matrix, and the horizontal axis is the aspect

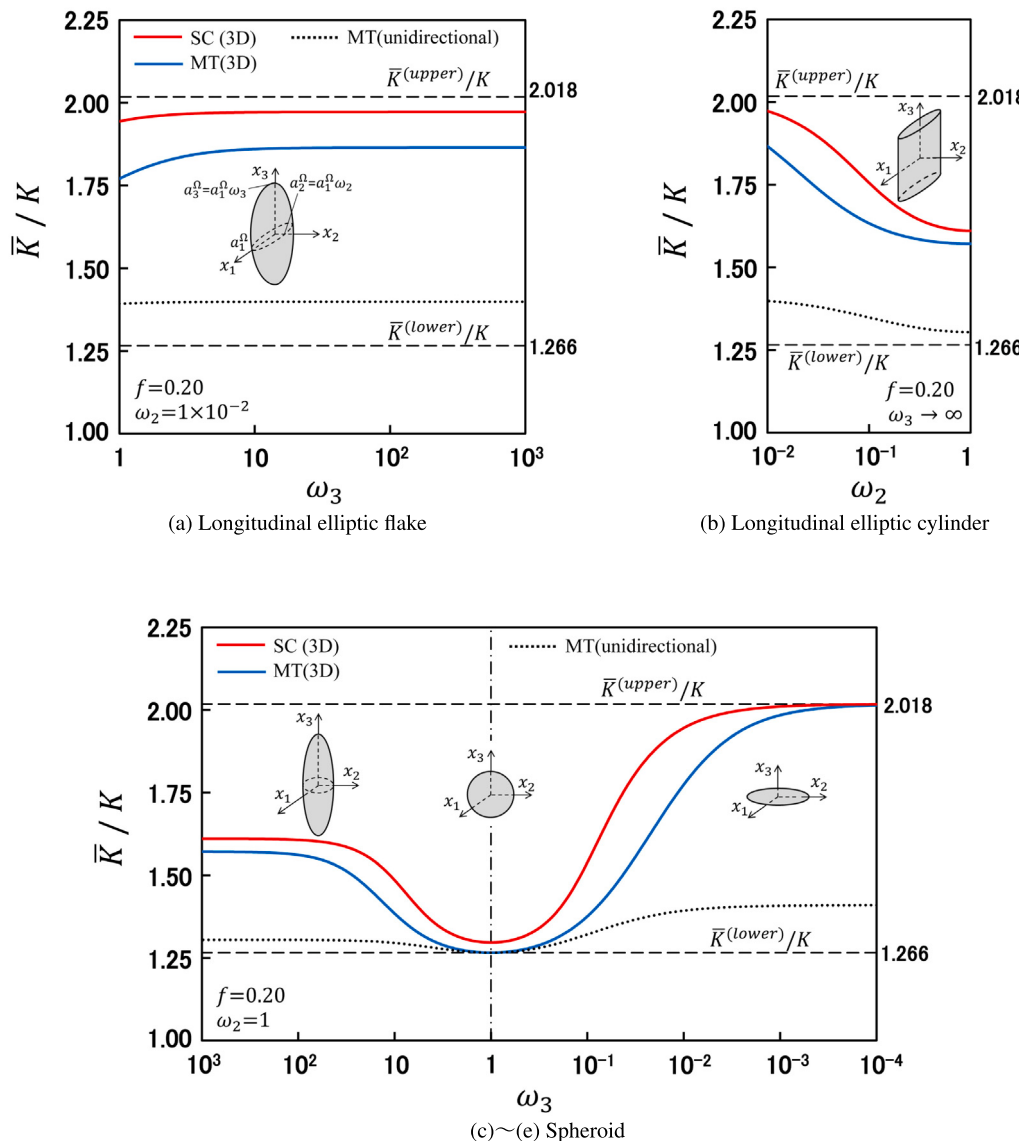


**Fig. 5.** Change in the effective bulk modulus of glass fillers/epoxy with the aspect ratio of the fillers. The solid red and blue lines are the results of the self-consistent method and the Mori-Tanaka method for the three-dimensional random orientation of the fillers, respectively. The dashed lines are the Hashin-Shtrikman's bounds, and the dotted line is the result of the Mori-Tanaka method for unidirectional orientation of the fillers. The effective bulk modulus indicated by the solid blue line, the dashed line, and the dotted line agrees with the lower bound when the shape of the fillers is spherical. The effective bulk modulus indicated by the solid red and blue lines approaches the upper bound as the shape of the fillers is thin oblate spheroidal.

ratio of the fillers. Figures (a) to (e) correspond to each shape in Fig. A.1. Furthermore, Hashin and Shtrikman's lower bound  $\bar{K}^{(lower)}$  and upper bound  $\bar{K}^{(upper)}$  for the effective bulk modulus of two-phase composites [6] are shown by the dashed lines. These solutions are given by

$$\bar{K}^{(lower)} = K_1 + \frac{f_2}{\frac{1}{K_2 - K_1} + \frac{3}{3K_1 + 4\mu_1} f_1}, \quad \bar{K}^{(upper)} = K_2 + \frac{f_1}{\frac{1}{K_1 - K_2} + \frac{3}{3K_2 + 4\mu_2} f_2}, \quad (K_1 < K_2, \mu_1 < \mu_2), \quad (69)$$

where  $K_i$ ,  $\mu_i$ , and  $f_i$  are bulk modulus, shear modulus, and volume fraction of the  $i$ th phase, respectively, and all phases are assumed to be isotropic materials. From the figure, it can be seen that the results of SC(3D) and MT(3D) always fall within the upper and lower bounds regardless of the shape of the fillers. In addition, as shown in Fig.(d), when the shape of the fillers is spherical ( $\omega_3 = 1$ ), the result of MT(3D) completely agrees with that of MT(unidirectional). This result is physically correct, since the shape of sphere is independent of orientation. The solution provided by the Mori-Tanaka method when the shape of the fillers is spherical is given by Eq. (46). Replacing with  $K \rightarrow K_1$ ,  $K^Q \rightarrow K_2$  and so on for  $\bar{K}$  in Eq. (46), and noting that  $f_1$  and  $f_2$  in Eq. (69) are the volume fractions of the matrix and the fillers, respectively, we find that  $\bar{K}$  in Eq. (46) agrees with the solution of the lower bound of Eq. (69). Therefore, when the shape of the fillers is spherical, MT(3D), MT(unidirectional), and the lower bound are completely identical. However, these results do not agree with SC(3D). When the shape of the fillers is oblate spheroidal, SC(3D) and MT(3D) asymptotically approach the upper bound as the value of  $\omega_3$  decreases. Additionally, it is interesting that the value of  $\bar{K}/K$  for the oblate spheroid ( $\omega_3 < 10^{-2}$ ) in Fig.(e) and the longitudinal elliptical flake in Fig.(a) is higher than that for the cylinder ( $\omega_2 = 1$ ) in Fig.(b) and the prolate spheroid ( $\omega_3 > 10^2$ ) in Fig.(c).

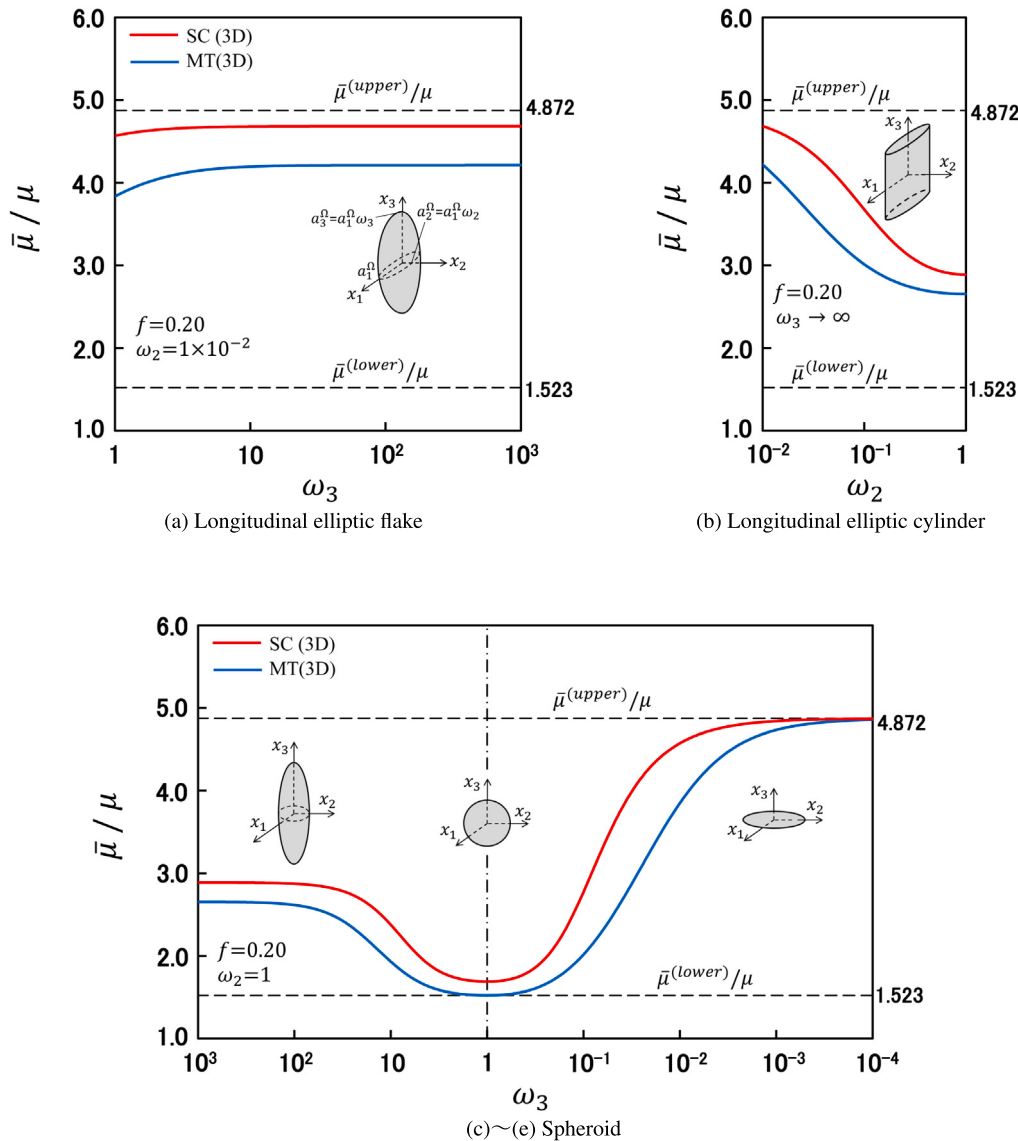


**Fig. 6.** Change in the effective shear modulus of glass fillers/epoxy with the aspect ratio of the fillers. The solid red and blue lines are the results of the self-consistent method and the Mori-Tanaka method for the three-dimensional random orientation of the fillers, respectively. The dashed lines are the Hashin-Shtrikman's bounds. The effective shear modulus indicated by the solid blue line and the dashed one agrees with the lower bound when the shape of the fillers is spherical. The effective shear modulus indicated by the solid red and blue lines approaches the upper bound as the shape of the fillers is thin oblate spheroidal.

Next, we consider the reason why the bulk modulus is higher in the case of oblate spheroid and elliptical flake than in the case of cylindrical shape. From the figure, it can be seen that MT(unidirectional) also has a similar tendency as MT(3D) and SC(3D). In the case of the cylindrical shape, the deformation of the whole material is suppressed only in the longitudinal direction of the filler, but in the case of oblate spheroid and elliptical flake, the deformation is suppressed simultaneously in any directions along the plane of the filler. Therefore, it is considered that the macroscopic volumetric strain decreases so that the bulk modulus increases in the case of oblate spheroids and elliptical flakes than in the case of cylindrical shape. In the case that the fillers are oriented randomly, this effect of the surface shape of the fillers is revealed in any direction, so the bulk modulus is higher than that in the case that the fillers are oriented unidirectionally.

Similar to Figs. 5, 6 shows the change in the effective shear modulus  $\bar{\mu}$  with the aspect ratio of the fillers. The line types in the figure are the same as those in Fig. 5, and the vertical axis in the figure is  $\bar{\mu}/\mu$ , which is dimensionless with the shear modulus  $\mu$  of the matrix. In the figure, Hashin and Shtrikman's lower bound  $\bar{\mu}^{(lower)}$  and upper bound  $\bar{\mu}^{(upper)}$  for the effective shear modulus of two-phase composites [6] are shown by the dashed lines. These solutions are given by

$$\bar{\mu}^{(lower)} = \mu_1 + \frac{f_2}{\frac{1}{\mu_2 - \mu_1} + \frac{6(K_1 + 2\mu_1)}{5\mu_1(3K_1 + 4\mu_1)} f_1} , \quad \bar{\mu}^{(upper)} = \mu_2 + \frac{f_1}{\frac{1}{\mu_1 - \mu_2} + \frac{6(K_2 + 2\mu_2)}{5\mu_2(3K_2 + 4\mu_2)} f_2} , \quad (K_1 < K_2, \mu_1 < \mu_2) . \quad (70)$$

From the figure, for  $\bar{\mu}$  as well as  $\bar{K}$ , it can be seen that the results of SC(3D) and MT(3D) always fall within the upper and lower bounds regardless of the shape of the fillers. Replacing with  $\mu \rightarrow \mu_1$ ,  $\mu^Q \rightarrow \mu_2$  and so on for  $\bar{\mu}$  in Eq. (46), this solution agrees with that of the lower bound in Eq. (70). Therefore, when the shape of the fillers is spherical, the solution of MT(3D) and the lower bound are identical, which is the similar result as  $\bar{K}$  in

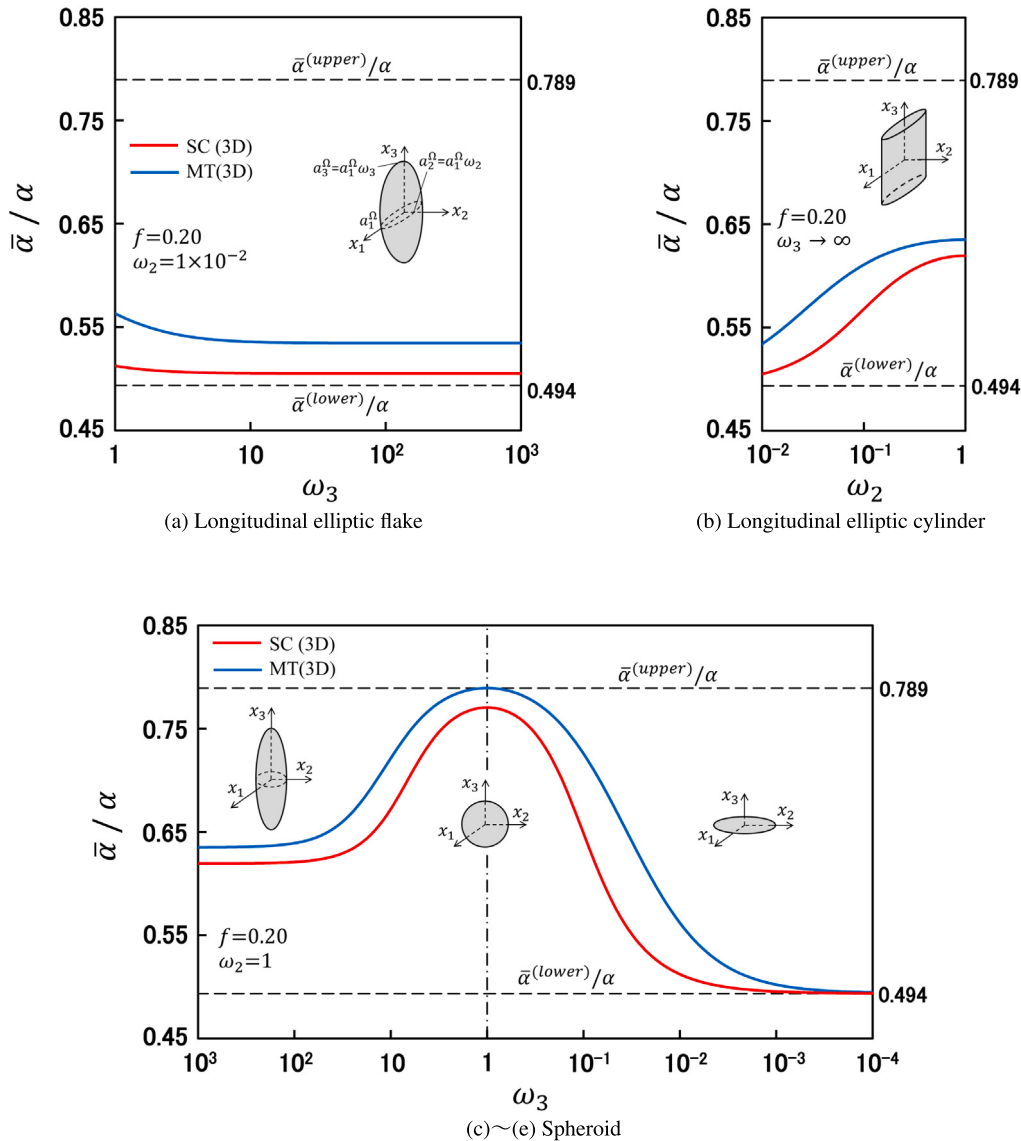


**Fig. 7.** Change in the effective thermal expansion coefficient of glass fillers/epoxy with the aspect ratio of the fillers. The solid red and blue lines are the results of the self-consistent method and the Mori-Tanaka method for the three-dimensional random orientation of the fillers, respectively. The dashed lines are the Rosen-Hashin's bounds. The effective thermal expansion coefficient indicated by the solid blue line and the dashed one agrees with the upper bound when the shape of the fillers is spherical. The effective thermal expansion coefficient indicated by the solid red and blue lines approaches the lower bound as the shape of the fillers is thin oblate spheroidal.

**Fig. 5.** In addition,  $\bar{\mu}$  for the oblate spheroid in Fig.(e) and longitudinal elliptical flake in Fig.(a) takes a higher value than that for the cylindrical shape, and this tendency is also consistent with that of  $\bar{K}$  in **Fig. 5**. Since the surface area of the oblate or flake shape is larger than that of the cylindrical one, the resistance to shear deformation in the case of the oblate or flake shape is expected to be greater than that in the case of the cylindrical one.

Similar to **Figs. 5** and **6**, **7** shows the change in the effective thermal expansion coefficient  $\bar{\alpha}$  with the aspect ratio of the fillers. The line types in the figure are the same as those in **Fig. 5**, and the vertical axis takes  $\bar{\alpha}/\alpha$  which is dimensionless with the thermal expansion coefficient  $\alpha$  of the matrix. Similar to Eqs. (69) and (70), Rosen and Hashin derived the lower bound  $\bar{\alpha}^{(lower)}$  and the upper bound  $\bar{\alpha}^{(upper)}$  for the effective thermal expansion coefficient of two-phase composites, which is indicated by dash lines in the figure [26]. These solutions are given by

$$\bar{\alpha}^{(lower)} = \alpha_1 - \frac{(\alpha_1 - \alpha_2)K_2(3K_1 + 4\mu_1)f_2}{K_1(3K_2 + 4\mu_1) + 4(K_2 - K_1)\mu_1 f_2}, \quad \bar{\alpha}^{(upper)} = \alpha_2 - \frac{(\alpha_2 - \alpha_1)K_1(3K_2 + 4\mu_2)f_1}{K_2(3K_1 + 4\mu_2) + 4(K_1 - K_2)\mu_2 f_1},$$

$$\left( \frac{\alpha_2 - \alpha_1}{K_2 - K_1} < 0, \mu_1 > \mu_2 \right), \quad (71)$$

where  $\alpha_i$  is the thermal expansion coefficient of the  $i$ th phase, and both phases are assumed to be isotropic materials. From the figure, it can be seen that the results of SC(3D) and MT(3D) always fall within the upper and lower bounds regardless of the shape of the fillers, similar to the results of the effective bulk modulus  $\bar{K}$  in **Fig. 5** and shear modulus  $\bar{\mu}$  in **Fig. 6**. Replacing  $\alpha \rightarrow \alpha_2$ ,  $\alpha^Q \rightarrow \alpha_1$ , and so on for  $\bar{\alpha}$  in Eq. (47), this solution agrees with that of the upper bound in Eq. (71). Therefore, when the shape of the fillers is spherical, the solution of MT(3D) and the upper bound are identical, which is the similar result as  $\bar{K}$  and  $\bar{\mu}$ . It can be seen that the value of  $\bar{\alpha}$  for the oblate spheroid in Fig.(e) and the longitudinal elliptic

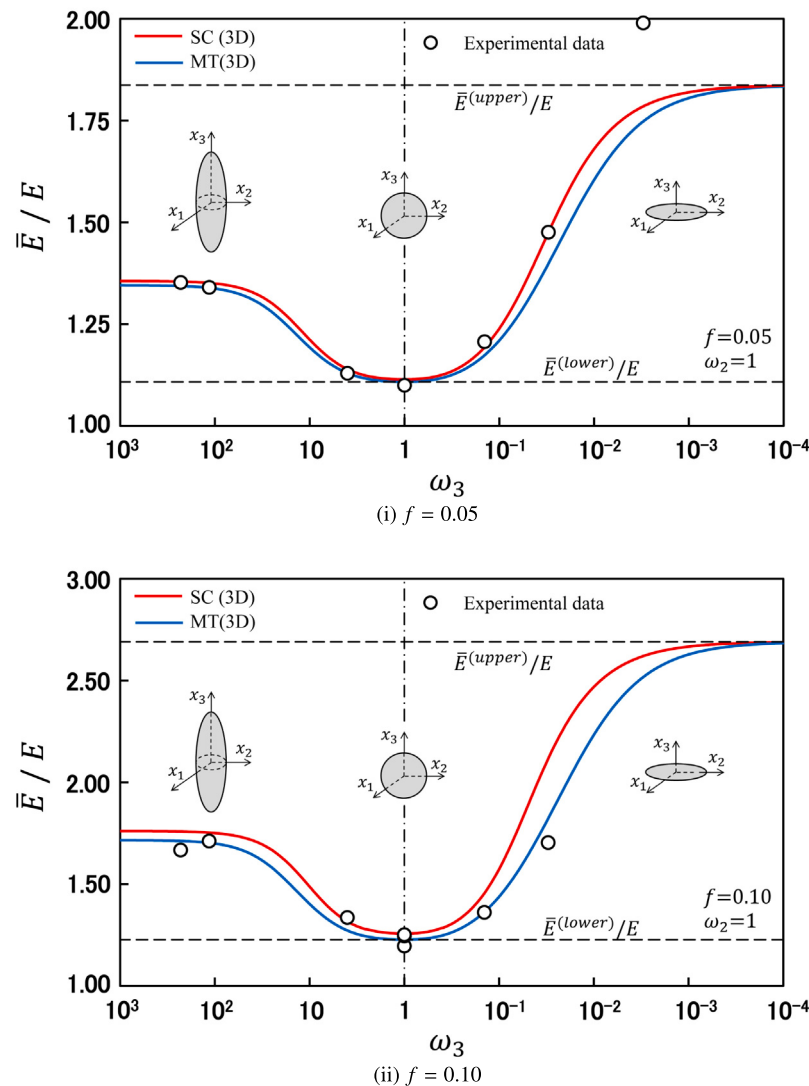


**Fig. 8.** Change in the effective Young's modulus of glass fillers/epoxy with the aspect ratio of spheroidal fillers. The solid red and the blue lines are the results of the self-consistent method and the Mori-Tanaka method for the three-dimensional random orientation of fillers, respectively. Open circles indicate experimental results obtained by Takahashi et al. [21].

flake in Fig.(a) is lower than that for other shapes. In the case of oblate spheroids and elliptic flakes, the thermal expansion of the whole material is suppressed simultaneously in any directions along the plane of the filler. As a result, the thermal expansion strain is reduced, so the effective thermal expansion coefficient is considered to be smaller than that in the case of cylindrical shape.

From the above results, it is confirmed that the analytical results of effective elastic moduli and the thermal expansion coefficient satisfy the condition that they must fall within the upper and lower bounds regardless of the shape of the fillers. In addition, it can be seen that there is a slight difference between the results of SC (3D) and MT (3D). This difference occurs by some constant amount in any shape of the fillers, and represents the difference in the evaluation of the interaction field between the SC (3D) and MT (3D). It is assumed that this difference increases as the volume fraction of the fillers increases. This will be discussed in comparison with experimental results in the next section.

#### 4.3. Comparison with experimental results

##### 4.3.1. Effective Young's modulus

In this section, we compare our analytical result of effective Young's modulus with the experimental one obtained by Takahashi et al. They produced plate-shaped and film-shaped specimens containing fillers with fibrous shape or flake one. The specimens are made by heating and stirring glass fillers and epoxy resin in a thermostatic bath, then pouring it into molds to cure. The fillers were randomly oriented in these specimens. They defined the following approximate equation for the effective Young's modulus when the volume fraction of the fillers is small:

$$\bar{E} = E(1 + c f),$$

where  $E$  is Young's modulus of the matrix,  $f$  is the volume fraction of the fillers, and  $c$  is called the Einstein coefficient. They experimentally obtained the change of the coefficient  $c$  with various aspect ratios of the filler. Here, the effective Young's modulus obtained by substituting this coefficient  $c$  into the above equation is compared with that obtained by our analysis.

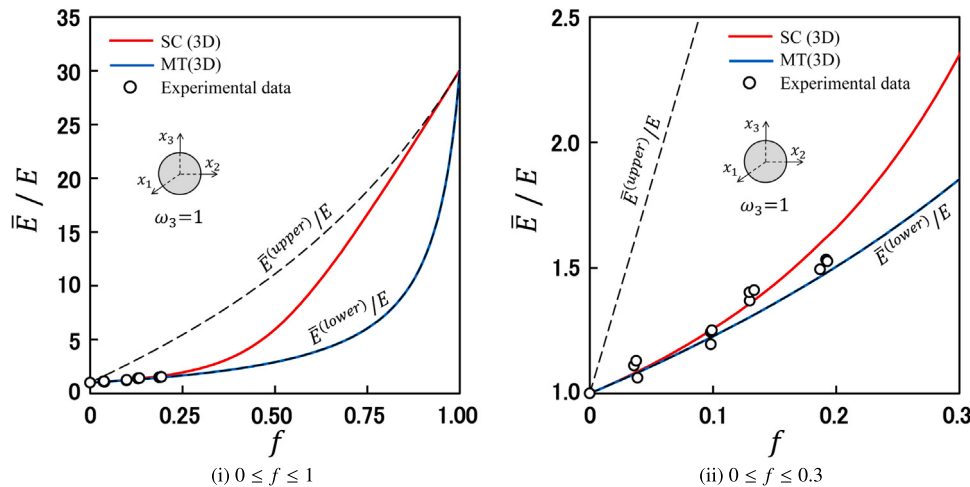


**Fig. 9.** Change in the effective Young's modulus of glass fillers/epoxy with the volume fraction of the fillers  $f$  when the shape of the fillers is spherical. Fig.(i) is for the case where the volume fraction of the fillers is  $0 \leq f \leq 1$ , and Fig.(ii) is an enlarged view of Fig.(i) for the range of  $0 \leq f \leq 0.3$ . The solid red and blue lines are the results of the self-consistent method and the Mori-Tanaka method respectively, and the dashed lines are the Hashin and Shtrikman's bounds. Open circles indicate experimental data obtained by Takahashi et al. [21].

Fig. 8 shows the changes in the effective Young's modulus  $\bar{E}$  with the aspect ratio  $\omega_3$  of the spheroidal filler. The material constants in Table 1 are used for this calculations. Fig. 8(i) shows the result when the volume fraction of the fillers is  $f = 0.05$ , and Fig. 8(ii) shows the result when  $f = 0.10$ . The solid red and blue lines in the figure are the results of SC (3D) and MT (3D) respectively, and the open circles are the experimental results for plate-shaped specimens obtained by Takahashi et al. The dashed lines in the figure represent the lower bound  $\bar{E}^{(lower)}$  and upper bound  $\bar{E}^{(upper)}$  of the effective Young's modulus, obtained from lower bounds  $\bar{K}^{(lower)}, \bar{\mu}^{(lower)}$  and upper bounds  $\bar{K}^{(upper)}, \bar{\mu}^{(upper)}$  obtained by Hashin et al. as shown in Eqs. (69) and (70).  $\bar{E}^{(lower)}$  and  $\bar{E}^{(upper)}$  are given by

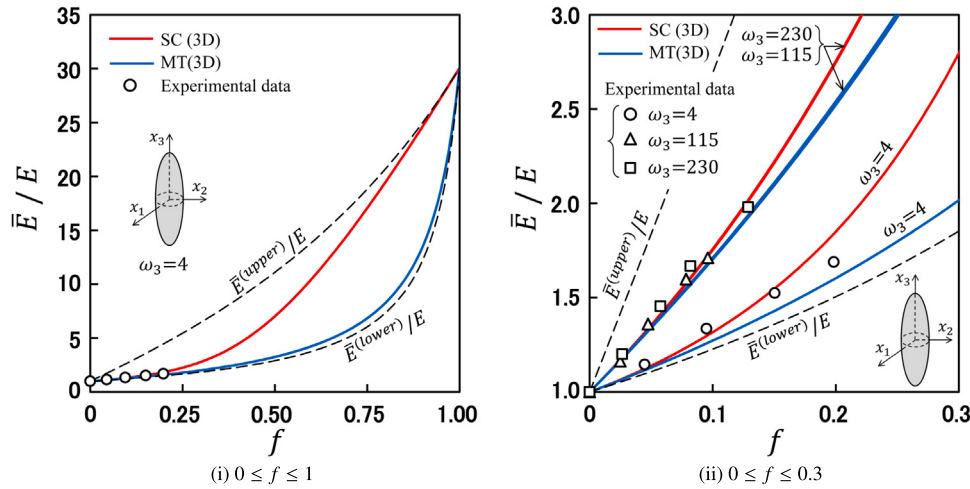
$$\bar{E}^{(lower)} = \frac{9\bar{K}^{(lower)}\bar{\mu}^{(lower)}}{\bar{\mu}^{(lower)} + 3\bar{K}^{(lower)}} , \quad \bar{E}^{(upper)} = \frac{9\bar{K}^{(upper)}\bar{\mu}^{(upper)}}{\bar{\mu}^{(upper)} + 3\bar{K}^{(upper)}} . \quad (72)$$

From Fig. 8(i), it can be seen that the result of SC(3D) agrees well with the experimental results for the oblate shape where  $\omega_3$  is less than 1, except for the experimental point of  $\omega_3 = 0.003$ . The reason for the large deviation from the experimental results for the extremely thin and flat shape at  $\omega_3 = 0.003$  will be explained later. In addition, both SC(3D) and MT(3D) agree well with experimental results for prolate spheroids with  $\omega_3$  greater than 1. On the other hand, in Fig. 8(ii), the result of MT(3D) seems to agree better with the experimental result than the result of SC(3D). In other words, we can see that the result of SC(3D) is overestimated. The reason for this will be examined in Section 4.4.

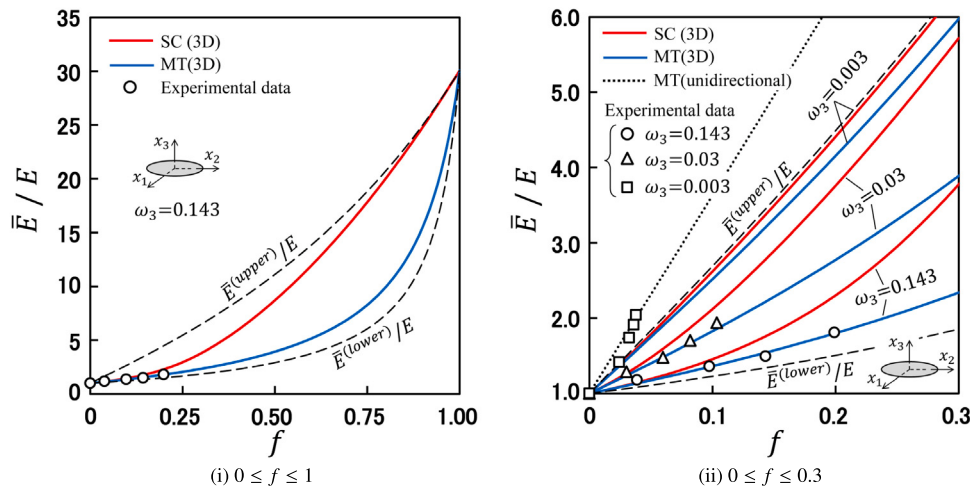
Fig. 9 shows the change in the effective Young's modulus  $\bar{E}/E$  with the volume fraction of the fillers  $f$  when the shape of the fillers is spherical. Fig. 9(i) is for the case where the volume fraction of the fillers is  $0 \leq f \leq 1$ , and Fig. 9(ii) is an enlarged view of Fig. 9(i) for the range of  $0 \leq f \leq 0.3$ . The line types and experimental points in the figure are the same as before. First, we compare the results of SC(3D) and MT(3D). From the figure, it can be seen that there is almost no difference between the results of SC(3D) and MT(3D) within the range of  $f$  being approximately less than 0.2. At  $f = 0.2$ , the difference between SC(3D) and MT(3D) is less than 10%. This result is consistent with the fact that although both methods use different approaches to evaluate the interaction between the fillers, they do not exhibit large discrepancies at low volume fraction of the fillers. Furthermore, as mentioned in Section 4.2, when the shape of the fillers is spherical, the result of MT(3D) coincides with that of the Hashin's lower bound, hence the two results in the figure perfectly overlap. Additionally, the result of SC(3D) falls within these two results, which also consistent with the generally expected observation. Next, we compare the results of SC(3D) and MT(3D) with experimental results. It can be seen that these analytical results are in good agreement with the experimental ones, although the experimental data points are only within  $f \leq 0.2$ .

Fig. 10 shows the results when the shape of the fillers is prolate spheroidal (fibrous shape). The line types, etc. in the figure are the same as in Fig. 9. Fig. 10(i) shows the results for case  $\omega_3 = 4$ . However, note that in Fig. 10(ii) the results for cases  $\omega_3 = 115$  and  $230$  are also presented. First, compare the results of SC(3D) and MT(3D). From Fig. 10(i), it can be seen that the behavior of SC(3D) and MT(3D) with increasing  $f$  is similar to the case of the sphere shown in Fig. 9(i). On the other hand, from Fig. 10(ii), it can be observed that the difference between SC(3D) and MT(3D) is smaller for the cases when  $\omega_3 = 115$  and  $230$  compared to the case when  $\omega_3 = 4$ . Next, comparing these analytical results with the experimental ones, there is a slight difference between them, and this difference is about 5% at most. Therefore, a good correlation can be seen between the analytical results and the experimental ones.

Fig. 11 shows the results when the shape of the fillers is oblate spheroidal (flake shape). In Fig. 11(ii), the results for  $\omega_3 = 0.143, 0.03$ , and  $0.003$  are shown. Similar to Fig. 10, there is a difference between SC(3D) and MT(3D), and this difference tends to decrease with decreasing  $\omega_3$ . Comparing these analytical results with the experimental ones, it is found that the results of MT(3D) agree better with the experimental results than the results of SC(3D) when  $\omega_3 = 0.143$  and  $0.03$ . We will discuss this reason in the next section. However, for  $\omega_3 = 0.003$ , the two analytical results deviate greatly from the experimental ones. According to the experimental results of Takahashi et al. they reported that it is difficult to mix uniformly and disperse randomly the fillers in the matrix resin, if the aspect ratio becomes extremely small and the shape of the fillers is very thin oblate. Since the specimens used in the experiment are plate-shaped, it is thought that the surface of the filler tends to be oriented along the plate surface when the shape of the fillers is thin oblate. Therefore, we perform calculations for the case where the oblate spheroidal fillers with  $\omega_3 = 0.003$  are oriented in one direction so that  $x_3$  axis is normal to the surface of the oblate spheroid. The result of the effective Young's modulus along the surface obtained by this calculation is shown by the dotted line in Fig. 11(ii). From the figure, it can be seen that this result agrees



**Fig. 10.** Change in the effective Young's modulus of glass fillers/epoxy with the volume fraction of the fillers  $f$  when the shape of the fillers is prolate spheroidal (fibrous shape). Fig.(i) is for the case where the volume fraction of the fillers is  $0 \leq f \leq 1$ , and Fig.(ii) is an enlarged view of Fig.(i) for the range of  $0 \leq f \leq 0.3$  and shows results for  $\omega_3 = 4, 115$ , and  $230$ . The solid red and blue lines are the results of the self-consistent method and the Mori-Tanaka method respectively, and the dashed lines are the Hashin and Shtrikman's bounds. Open circles, triangles, and squares indicate experimental data obtained by Takahashi et al. [21].



**Fig. 11.** Change in the effective Young's modulus of glass fillers/epoxy with the volume fraction of the fillers  $f$  when the shape of the fillers is oblate spheroidal (flake shape). Fig.(i) is for the case where the volume fraction of the fillers is  $0 \leq f \leq 1$ , and Fig.(ii) is an enlarged view of Fig.(i) for the range of  $0 \leq f \leq 0.3$  and shows results for  $\omega_3 = 0.143, 0.03$ , and  $0.003$ . The solid red and blue lines are the results of the self-consistent method and the Mori-Tanaka method respectively, and the dashed lines are the Hashin and Shtrikman's bounds. Open circles, triangles, and squares indicate the experimental data obtained by Takahashi et al. [21].

well with the experimental results indicated by the open squares. From this result, the reason for the deviation of the analytical results from the experimental point when  $\omega_3 = 0.003$  in Fig. 8(i) is considered to be that the distribution of the fillers becomes close to be unidirectional orientation.

In Fig. 11(ii), it is found that the results of MT(3D) agree better with the experimental results than the results of SC(3D) when  $\omega_3 = 0.143$  and  $0.03$ . A similar tendency is also seen in Fig. 8(ii). Takahashi et al. reported that it was difficult to defoam when the volume fraction of the fillers was more than 0.1. In other words, the existence of voids in the material is considered to be the reason why the experimental results of the effective Young's modulus take lower values than the analytical results. In Section 4.4, we will consider the case where voids also exist in the material.

Okuno investigated the effect of the aspect ratio of mica fillers on the effective Young's modulus of materials containing mica fillers in polypropylene resin matrix. He made fillets by melting and mixing matrix resin and fillers, applied a silane coupling agent to them, and then processed them into plate-shaped test specimens by injection molding. It was confirmed that the mica fillers were randomly oriented within the material.

Fig. 12 shows the change in the effective Young's modulus  $\bar{E}$  of the material with the volume fraction of mica fillers. Fig. 12 performs the same comparison as Fig. 11(ii). The line styles in the figure are the same as Fig. 11. Additionally, the open circles, squares, and triangles in the figure represent experimental results obtained by Okuno, corresponding to results for  $\omega_3 = 0.0615, 0.0357$ , and  $0.0261$ , respectively. Comparing the results of SC(3D) and MT(3D) with the experimental results, the results of SC(3D) are closer to the experimental results than those of MT(3D), with an average error of about 8%.

#### 4.3.2. Effective thermal expansion coefficient

Miya et al. experimentally evaluated the effective thermal expansion coefficient of composite materials containing spheroidal short glass fibers in epoxy resin. In the experiment, they suspended glass fibers cut to a predetermined length in distilled water, and then created a mat with fibers

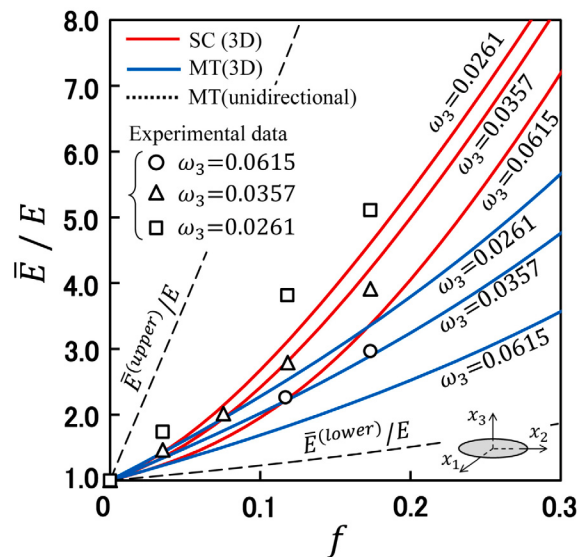


**Fig. 12.** Change in the effective Young's modulus of phlogopite mica fillers/polypropylene with the volume fraction of the fillers  $f$  when the shape of the fillers is oblate spheroidal (flake shape). The figure shows the results for aspect ratios of the fillers  $\omega_3 = 0.0615, 0.0357$ , and  $0.0261$ . The solid red and blue lines are the results of the self-consistent method and the Mori-Tanaka method respectively, and the dashed lines are the Hashin and Shtrikman's bounds. Open circles, triangles, and squares indicate the experimental data obtained by Okuno [22].

randomly oriented in two dimensional by sedimentation onto filter paper. This mat was then impregnated with resin in a vacuum chamber to produce cylindrical test specimens. The axis of the cylindrical test specimens aligned with the direction of random fiber orientation. Miwa et al. determined the thermal expansion coefficient of the material in this axial direction. They prepared test specimens with various aspect ratios of the fibers and experimentally evaluated the effect of fiber aspect ratio on the effective thermal expansion coefficient of the material. The volume fraction of the fibers was kept constant at 6% for all test specimens. Additionally, Miwa et al. focused on the temperature dependency of the elastic constants and thermal expansion coefficients of the resin, investigating its effect on the effective thermal expansion coefficient. To compare with experimental results, the material constants in Table 3 are used for calculations.

Fig. 13 illustrates the change in the effective thermal expansion coefficient  $\bar{\alpha}$  with the aspect ratio of spheroidal glass fillers. Figures 13(i), (ii), and (iii) represent results at temperatures of  $T = 20^\circ\text{C}$ ,  $40^\circ\text{C}$ , and  $60^\circ\text{C}$ , respectively. The line styles in the figure are the same as those in Fig. 7. The open circles represent the experimental data of Miwa et al. It should be noted that the value of the elastic moduli and the thermal expansion coefficient of the matrix vary with temperature, as shown in Table 3. From Fig. 13(i), (ii), (iii), it is evident that SC(3D) and MT(3D) exhibit behavior similar to those shown in Fig. 7, since the constituents of materials used in Figs. 7 and 11 are the same. Moreover, the results of SC(3D) and MT(3D) generally align with the experimental results. Therefore, the validity of this analytical solution for the case of spheroidal fillers has been demonstrated.

#### 4.4. Investigation for the coexistence of fillers and voids in materials

In this section, by using the solution obtained in Chap.3, we calculate the effective Young's modulus of the material in which fillers and voids coexist. Fig. 14(c) and (e) show the analytical results of the effective Young's modulus  $\bar{E}/E$  with the volume fraction of the fillers  $f$  for the cases where the shape of the fillers is an oblate spheroid with  $\omega_3 = 4$  and a prolate spheroid with  $\omega_3 = 0.143$ , respectively, with the void volume fraction  $f_{void}$  as a parameter. The results for  $f_{void} = 0$  correspond to those shown in Figs. 10 and 11. In addition, the experimental results obtained by Takahashi et al. are also indicated by open circles. From these figures, regardless of the value of  $f$ , the results of SC(3D) and MT(3D) decrease as  $f_{void}$  increases. Since the elastic modulus of the void is zero, it is obvious that the effective Young's modulus decreases as the volume fraction of the voids increases. From Fig. 14(c), when comparing the results of SC(3D) with the experimental results, it is evident that the result of SC(3D) with  $f_{void} = 0.025$  shows a good agreement with the experimental data at the point where  $f = 0.2$ . On the other hand, from Fig. 14(e), it can be observed that the results of SC(3D) with  $f_{void} = 0.025, 0.050$ , and  $0.075$  are in good agreement with the experimental data at  $f = 0.1, 0.15$ , and  $0.20$ , respectively. Based on the above results, it is speculated that the reason why the experimental results in Figs. 8(ii) and 11(ii) are closer to MT(3D) than SC(3D) when  $f > 0.1$  is due to the presence of voids within the material. Although the amount of vacancies is not clarified in Takahashi et al.'s experiment, it is thought that the problem pointed out by Takahashi et al. can be explained to some extent by the results of our analysis. Since voids can be regarded as a type of filler, it is expected that our analytical methods can be applied to actual materials that contain many types of fillers.

#### 4.5. Effects of surface area and projected area of fillers on effective elastic properties

As can be seen from Figs. 5 to 7, the effective elastic properties may take the same value even if the aspect ratio of the filler is different. For example, when the value of the aspect ratio  $\omega_3$  is about 10 and  $10^{-1}$ ,  $\bar{K}/K$  takes the same value of approximately 1.5, according to the result of the self-consistent method. From these results, it can be seen that the effective elastic properties are not uniquely determined by only the aspect ratio. Therefore, we investigate the shape parameters of the filler that uniquely determine the effective elastic properties. As mentioned in the discussion of these results, the effective elastic properties show characteristic values when the shape of the fillers is an extremely thin flake. The reason for this is considered to be the effect of the surface area of the flake-like filler. We will investigate this effect in detail.

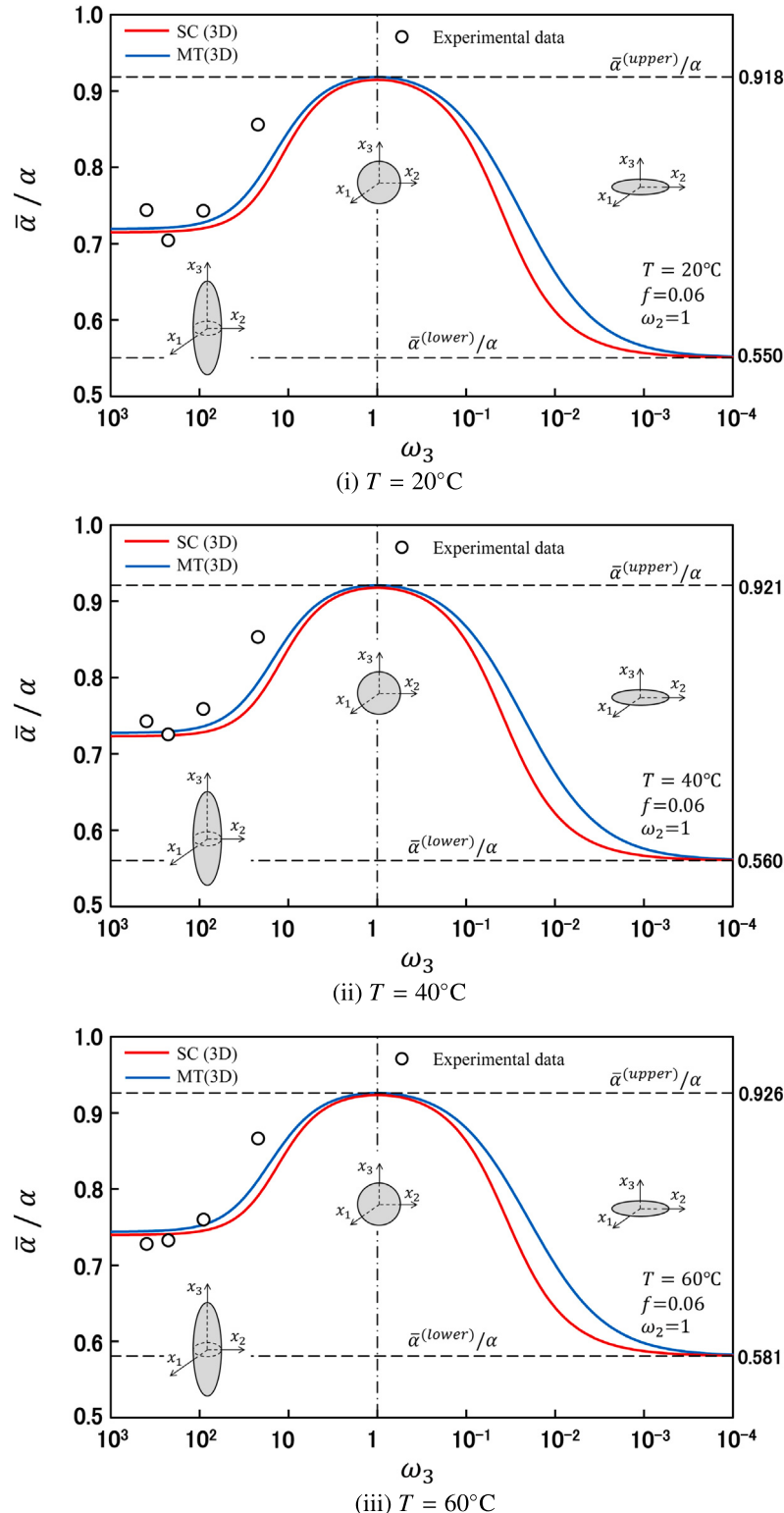


**Fig. 13.** Change in the effective thermal expansion coefficient of glass fillers/epoxy with the aspect ratio of the spheroidal fillers. The solid red and blue lines are the results of the self-consistent method and the Mori-Tanaka method for the three-dimensional random orientation of the fillers, respectively. The dashed lines are the Rosen-Hashin's bounds. Open circles indicates the experimental data obtained by Miwa et al. [23].

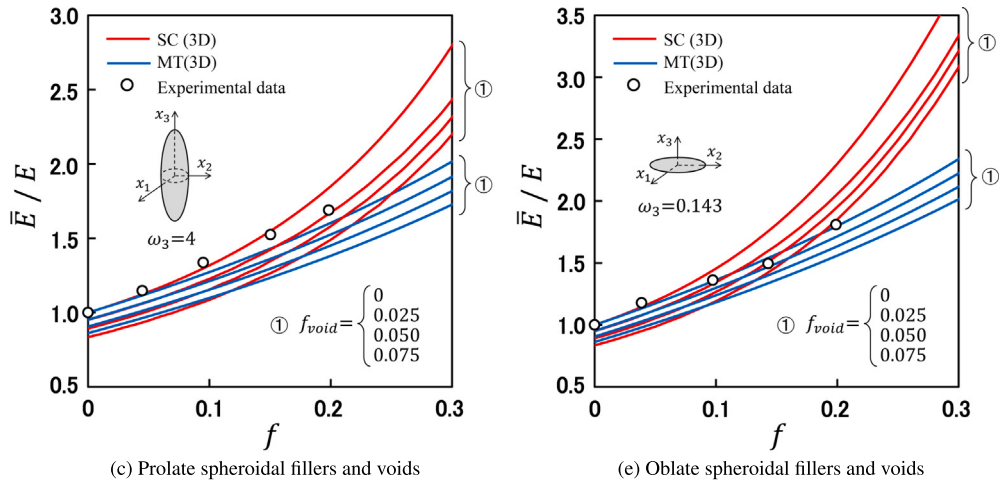


**Fig. 14.** Change in the effective Young's modulus of glass fillers/epoxy with the volume fraction of the fillers  $f$  when the material contains not only fillers but also voids. Fig.(c) is for the case where the shape of the fillers is prolate spheroidal (fibrous,  $\omega_3 = 4$ ), and Fig.(e) for the case where the shape of the fillers is oblate spheroidal (flake,  $\omega_3 = 0.143$ ). In both figures, the shape of the voids is sphere ( $\omega_3 = 1$ ). The volume fraction of voids  $f_{void}$  is used as a parameter. The solid red and blue lines are the results of the self-consistent method and the Mori-Tanaka method respectively. Open circles indicate experimental data obtained by Takahashi et al. [21].

Now, let the reference shape of the filler be a sphere. Consider an ellipsoidal filler with the same volume as this spherical filler. If the radius of the spherical filler is  $a$  and the length of the major semiaxis of the ellipsoidal filler is  $a_i (a_3 > a_1 > a_2)$ , then the radius of the spherical filler is given by  $a = (a_1 a_2 a_3)^{1/3}$ .

The ratio of the surface area of the ellipsoidal filler to the surface area of the spherical one is defined as  $r_{as}$ . Using the aspect ratios  $\omega_3 = a_3/a_1$  and  $\omega_2 = a_2/a_1$ ,  $r_{as}$  is expressed as follows:

$$r_{as} = \frac{1}{2(\omega_2 \omega_3)^{\frac{2}{3}}} \left\{ (\omega_2)^2 + \frac{\omega_2^2}{\sqrt{\omega_3^2 - \omega_2^2}} F(\theta, k) + \sqrt{\omega_3^2 - \omega_2^2} E(\theta, k) \right\}, \quad (\text{ellipsoid}) \quad , \quad (73a)$$

where,  $F(\theta, k)$  and  $E(\theta, k)$  are incomplete elliptic integrals of the first and second kind, respectively, and are given as follows:

$$F(\theta, k) = \int_0^\theta \frac{1}{\sqrt{1 - k^2 \sin^2 \omega}} d\omega, \quad E(\theta, k) = \int_0^\theta \sqrt{1 - k^2 \sin^2 \omega} d\omega, \quad (74a)$$

$$k = \sqrt{\frac{1 - \omega_2^2}{1 - \left(\frac{\omega_2}{\omega_3}\right)^2}}, \quad \theta = \sin^{-1} \sqrt{1 - \left(\frac{\omega_2}{\omega_3}\right)^2}. \quad (74b)$$

In particular, in the case of a prolate spheroid and an oblate spheroid,  $r_{as}$  in Eq. (73a) reduces to the following equations.

$$r_{as} = \frac{1}{2\omega_3^{\frac{2}{3}}} \left\{ 1 + \frac{\omega_3^2}{\sqrt{1 - \omega_3^{-2}}} \sin^{-1} \sqrt{1 - \omega_3^{-2}} \right\}, \quad (\text{prolate spheroid}), \quad (73b)$$

$$r_{as} = \frac{1}{2\omega_3^{\frac{2}{3}}} \left\{ 1 + \frac{\omega_3^2}{\sqrt{1 - \omega_3^2}} \tanh^{-1} \sqrt{1 - \omega_3^2} \right\}, \quad (\text{oblate spheroid}). \quad (73c)$$

**Fig. 15** combines the three figures ((a), (b), and (c)~(e)) shown for each of **Figs. 5 to 7** into one comprehensive figure by using the ratio of surface area  $r_{as}$ . The horizontal axis of the figure is  $r_{as}$ , and the vertical axes of **Fig. 15(i)**, (ii), and (iii) are the effective bulk elastic modulus  $\bar{K}$ , the shear modulus  $\bar{\mu}$ , and the thermal expansion coefficient  $\bar{\alpha}$ . The red and blue lines in the figure are the results of SC(3D) and MT(3D) as before. These results classify line types according to the shape of the filler; dashed lines represent the results for longitudinal elliptic flakes, dotted lines for prolate ellipsoids, and solid lines for oblate spheroids. Additionally, blue and red circular points in the figure represent results for spherical fillers. Black dashed lines indicate the results of upper and lower bounds. Note that the longitudinal elliptic cylinder shown in **Figs. 5(b), 6(b)** and **7(b)** has  $\omega_3 \rightarrow \infty$  and its surface area is infinite, so it is not shown in **Fig. 15**. **Fig. 15(i)** and (ii) show that, regardless of the shape of the fillers, as  $r_{as}$  increases, the effective elastic moduli  $\bar{K}$  and  $\bar{\mu}$  increase. Also, from these results, it can be seen that the results for the solid line (oblate spheroid) are higher than that for the dotted line (prolate spheroid) over the entire range of  $r_{as}$ . The result of the thermal expansion coefficient  $\bar{\alpha}$  in **Fig. 15(iii)** has a tendency opposite to these results. Therefore, it can be seen that  $r_s$  cannot uniquely determine the effective elastic properties of a material. This suggests that other geometric factors besides surface area also influence effective properties.

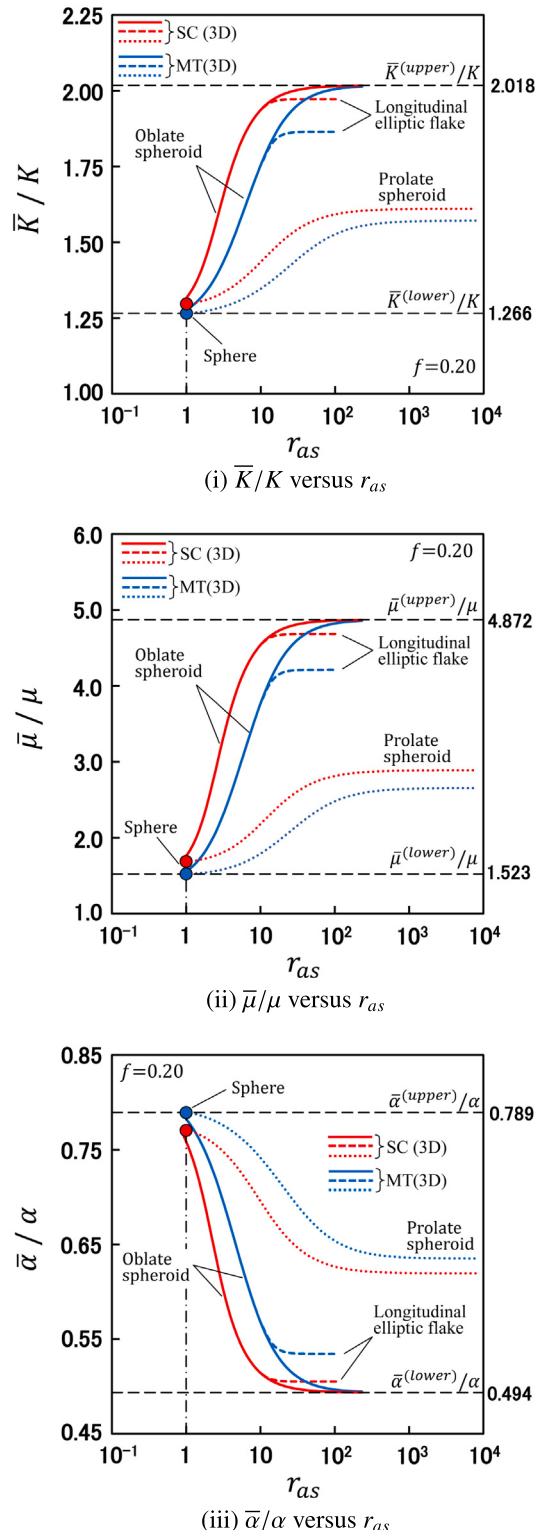


**Fig. 15.** Change in the effective bulk modulus  $\bar{K}/K$ , shear modulus  $\bar{\mu}/\mu$ , and thermal expansion coefficient  $\bar{\alpha}/\alpha$  with the ratio of surface area  $r_{as}$ . The red and blue lines are the results of the self-consistent method and the Mori-Tanaka method, respectively. For each method, the solid lines represent the results for oblate spheroids, the dashed lines for longitudinal elliptic flakes, and the dotted lines for prolate spheroids.

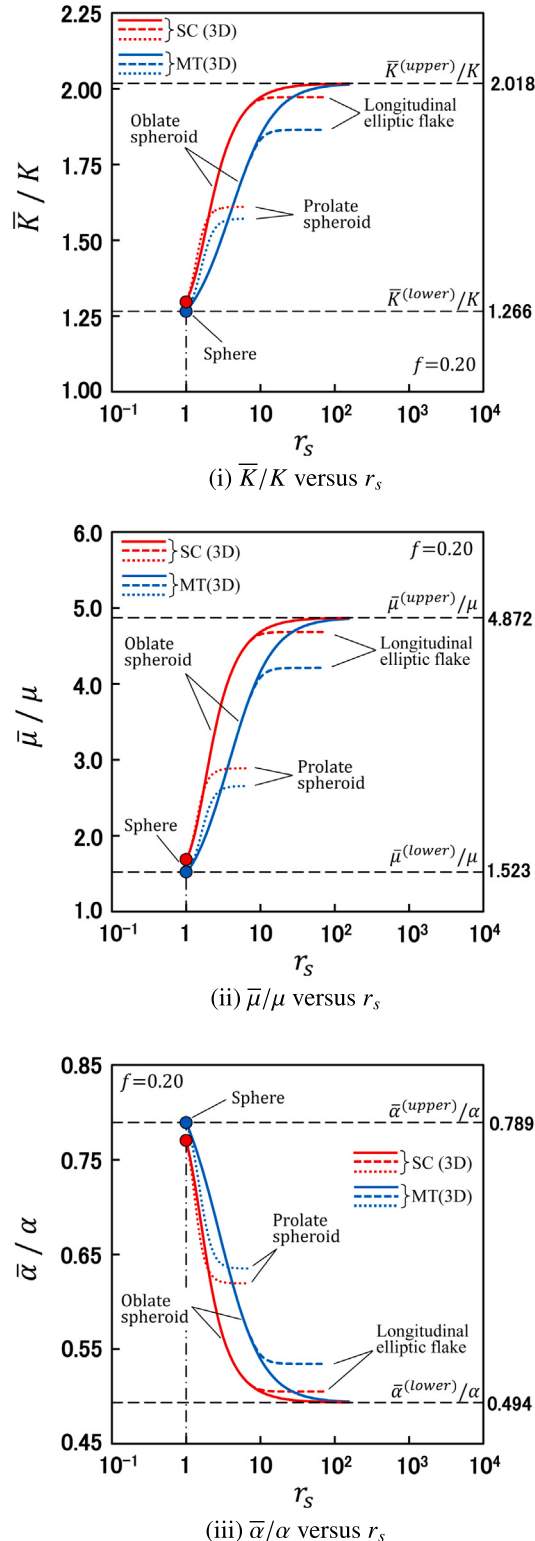


**Fig. 16.** Change in the effective bulk modulus  $\bar{K}/K$ , shear modulus  $\bar{\mu}/\mu$ , and thermal expansion coefficient  $\bar{\alpha}/\alpha$  with the shape factor  $r_s$ . The red and blue lines are the results from the self-consistent method and the Mori-Tanaka method, respectively. For each method, the solid lines represent the results for oblate spheroids, the dashed lines for longitudinal elliptic flakes, and the dotted lines for prolate spheroids.

Let the surface area of the ellipsoid be  $S$ , and the average value of the projected area on the  $x_1$ ,  $x_2$ , and  $x_3$  planes be  $\bar{S}^p$ . Then, we can set  $r_{fs} = \bar{S}^p/S$ . In the case of an ellipsoid,  $r_{fs}$  is as follows.

$$r_{fs} = \frac{\omega_2 + \omega_3 + \omega_2 \omega_3}{6 \left\{ (\omega_2)^2 + \frac{\omega_2^2}{\sqrt{\omega_3^2 - \omega_2^2}} F(\theta, k) + \sqrt{\omega_3^2 - \omega_2^2} E(\theta, k) \right\}}, \quad (\text{ellipsoid}) \quad (75a)$$

In the case of a spheroid,  $r_{fs}$  is as follows.

$$r_{fs} = \frac{1 + 2\omega_3}{6 \left\{ 1 + \frac{\omega_3^2}{\sqrt{1 - \omega_3^{-2}}} \sin^{-1} \sqrt{1 - \omega_3^{-2}} \right\}}, \quad (\text{prolate spheroid}), \quad (75b)$$

$$r_{fs} = \frac{1 + 2\omega_3}{6 \left\{ 1 + \frac{\omega_3^2}{\sqrt{1 - \omega_3^2}} \tanh^{-1} \sqrt{1 - \omega_3^2} \right\}}, \quad (\text{oblate spheroid}). \quad (75c)$$

In the discussion of Figs. 5 and 6, it is considered that since flake-like fillers have a flat surface, the effective elastic moduli increases in any direction within the plane. Now, we define a new factor  $r_{fs}$  that represents the ease with which a flat surface appears.

The product of  $r_{as}$  in Eq. (73) and  $r_{fs}$  in Eq. (75) is a factor that represents the degree of flat surface area when compared to a sphere with the same volume. To make this factor equal to 1 for a sphere, the product of  $r_{as}$  and  $r_{fs}$  is further multiplied by 4. We will define this as  $r_s$  and refer to it as the shape factor.  $r_s$  is given as follows, regardless of the shape of the ellipsoidal filler.

$$r_s = 4r_{as} r_{fs} = \frac{\omega_2 + \omega_3 + \omega_2 \omega_3}{3(\omega_2 \omega_3)^{\frac{2}{3}}}. \quad (76)$$

$r_s$  in the case of a spheroid can be obtained by substituting 1 for  $\omega_2$  in Eq. (76). Fig. 16 shows the results when the horizontal axis in Fig. 15 is replaced with the shape factor  $r_s$  determined by Eq. (76). When compared with Fig. 15, it can be seen that all the curves in Fig. 16 tend to converge and gather into a single curve. From this, we can find that the ease of occurrence of flat surface shapes, considering not only surface area but also projected area, is closely related to the effective elastic properties of the material. Therefore, selecting shapes of fillers that maximize the shape factor  $r_s$  would lead to an expected improvement in effective elastic moduli. This fact can be expected to hold without restricting the shape of the fillers to an ellipsoid.

## 5. Conclusions

In this study, the effective bulk modulus, shear modulus, and thermal expansion coefficient of the composite material containing ellipsoidal fillers oriented randomly in the material are explicitly derived by using the self-consistent method and the Mori-Tanaka method. These solutions can be expressed by common coefficients composed both of the physical properties of constituents and the geometrical factors of the filler. It is confirmed that these solutions are consistent because they include the solutions for the case where the shape of the fillers is spherical. Furthermore, by using these solutions, we can solve explicitly the effective elastic moduli and the thermal expansion coefficient both for the composite material and the polycrystal in which the various types of fillers (or crystal grains) with different shapes and physical properties are oriented randomly. Using these solutions, we calculate the change in the effective elastic moduli and the thermal expansion coefficient with changing continuously the shape of the fillers. From this result, we confirm that the results of these effective properties fall within the upper and lower bounds regardless of the shape of the fillers, indicating their consistency from an energy standpoint. When the elastic moduli of the filler are higher than that of the matrix, interesting results are obtained that the value of effective elastic moduli when the shape of the fillers is oblate or flake is higher than that when the shape of the fillers is cylindrical. In addition, our analytical results exhibit quantitative agreement with experimental ones. From the above, it is shown that our analytical solutions are valid and applicable to actual materials. Furthermore, based on these results, we define the shape factor that can represent both the degree of the surface area relative to the volume of the filler and the degree of the projected area of the filler along each axis. We can show that this factor has the potential to provide guidelines for the optimal design of filler shape to improve the effective elastic properties of materials.

In this study, the physical properties of fillers are assumed to be isotropic. However, in cases where the shape of the fillers is fibrous or flake-like, the physical properties of the filler often become anisotropic. For instance, carbon fibers, widely used as reinforcements in composite materials, exhibit significant differences in elastic moduli along the fiber axis and perpendicular to it. Therefore, it is important to derive a solution that takes into account the anisotropy of the fillers. The coefficients used in the solutions derived in this analysis are separated clearly into terms related to the physical properties and shape of the filler, serving as a guide for deriving solutions for cases where the physical properties of fillers are anisotropic. Additionally, in the analytical model used in this study, it is assumed that the filler and matrix are completely bonded at their interface. Surface treatments such as applying coupling agents to the filler's surface are common practices to improve adhesion between the filler and the matrix, so this assumption does not compromise generality. However, it is evident that the presence of a distinct interfacial layer with a thickness and different properties from the filler and matrix cannot be ignored. Therefore, deriving general solutions for cases where fillers have such interfacial layers will be a subject of future investigation.

## CRediT authorship contribution statement

**Hiroyuki Ono:** Conceptualization, Data curation, Formal analysis, Funding acquisition, Investigation, Methodology, Project administration, Resources, Software, Supervision, Validation, Visualization, Writing – original draft, Writing – review & editing.

## Declaration of competing interest

The authors declare the following financial interests/personal relationships which may be considered as potential competing interests: Hiroyuki ONO reports financial support was provided by Kyoto Institute of Technology.

## Data availability

Data will be made available on request.

## Appendix. Eshelby's tensor and coefficients in expressions

### A.1. Eshelby's tensor expressed in terms of the geometrical factors

The Eshelby's tensor is expressed in terms of the geometrical dimensions of the ellipsoidal filler and the Poisson's ratio  $\nu$  of the matrix. Mura provides a comprehensive summary of the Eshelby's tensor for various shapes of filler such as sphere and cylinder in his book [15], and expresses the Eshelby's tensor using two types of coefficients, which involve incomplete elliptic integrals of the first and second kinds. However, one of these coefficients has a dimension of 1/length squared, which prevents the Eshelby's tensor from being expressed in a regular form with respect to the aspect ratios of the ellipsoidal filler and the Poisson's ratio of the matrix. As a result, this form of the Eshelby's tensor is not suitable for analyses in which the shape of the fillers continuously changes by varying the aspect ratio.

To overcome this limitation, Araki et al. gave the Eshelby's tensor  $S_{ijkl}^{\Omega}$  for the ellipsoidal filler using coefficients  $H_i^{\Omega}$  and  $H_{ij}^{\Omega}$ , which consist of only aspect ratios of the filler, as follows [20].

$$\begin{aligned} S_{1111}^{\Omega} &= H_1^{\Omega} + \frac{1}{2(1-\nu)} \{ (H_1^{\Omega} - H_{12}^{\Omega}) + (H_3^{\Omega} - H_{31}^{\Omega}) \} , \\ S_{1122}^{\Omega} &= \frac{\nu}{1-\nu} H_1^{\Omega} - \frac{1}{2(1-\nu)} (H_1^{\Omega} - H_{12}^{\Omega}) , \\ S_{2211}^{\Omega} &= \frac{\nu}{1-\nu} H_2^{\Omega} - \frac{1}{2(1-\nu)} (H_1^{\Omega} - H_{12}^{\Omega}) , \\ S_{1212}^{\Omega} &= \frac{1}{2} (H_1^{\Omega} + H_2^{\Omega}) - \frac{1}{2(1-\nu)} (H_1^{\Omega} - H_{12}^{\Omega}) . \end{aligned} \quad (\text{A.1})$$

$H_i^{\Omega}$  and  $H_{ij}^{\Omega}$  are referred to as the geometrical factors. The other components are obtained by circularly permuting the subscripts (1, 2, 3) on both sides of equations. The components that cannot be obtained by circular permutation are zero.  $H_i^{\Omega}$  and  $H_{ij}^{\Omega}$  are given by the following equations using the aspect ratios  $\omega_3 = a_3^{\Omega}/a_1^{\Omega} > 1$  and  $\omega_2 = a_2^{\Omega}/a_1^{\Omega} < 1$  for an ellipsoid with principal semi-axis lengths  $a_3^{\Omega} > a_1^{\Omega} > a_2^{\Omega}$ .

$$\begin{aligned} H_3^{\Omega} &= \frac{\omega_3 \omega_2}{(\omega_3^2 - 1)(\omega_3^2 - \omega_2^2)^{1/2}} \{ F(\theta, k) - E(\theta, k) \} , \quad H_2^{\Omega} = \frac{1}{1 - \omega_2^2} \left\{ 1 - \frac{\omega_3 \omega_2 E(\theta, k)}{(\omega_3^2 - \omega_2^2)^{1/2}} \right\} , \\ H_3^{\Omega} + H_1^{\Omega} + H_2^{\Omega} &= 1 , \\ H_{31}^{\Omega} &= \frac{1}{\omega_3^2 - 1} (H_1^{\Omega} - H_3^{\Omega}) , \quad H_{12}^{\Omega} = \frac{\omega_2^2}{1 - \omega_2^2} (H_2^{\Omega} - H_1^{\Omega}) , \quad H_{23}^{\Omega} = \frac{\omega_3^2}{\omega_2^2 - \omega_3^2} (H_3^{\Omega} - H_2^{\Omega}) , \end{aligned} \quad (\text{A.2})$$

where  $F(\theta, k)$  and  $E(\theta, k)$  are the incomplete elliptic integrals of the first and second kinds, respectively, and  $\theta$  and  $k$  are given as

$$\theta = \sin^{-1} \left( 1 - \frac{\omega_2^2}{\omega_3^2} \right)^{\frac{1}{2}} , \quad k = \sqrt{\frac{\omega_3^2 - 1}{\omega_3^2 - \omega_2^2}} . \quad (\text{A.3})$$

Fig. A.1 shows various shapes of ellipsoidal filler  $\Omega$ . Fig.A(a) is called a longitudinal elliptic flake, which is thin in the  $x_2$  direction and elongated in the  $x_3$  direction. Fig.A(b) is called a longitudinal elliptic cylinder extended infinitely along the  $x_3$  axis, and the cross-sectional shape in the  $x_1-x_2$  plane is an ellipse. Fig.A(c) is a prolate spheroid whose longitudinal direction is the  $x_3$  axis, Fig.A(d) is a sphere and Fig.A(e) is an oblate spheroid and thin in the direction of the  $x_3$  axis. The nonzero components of the geometrical factors  $H_i$  and  $H_{ij}$  for these ellipsoidal shapes are expressed as

(a) Longitudinal elliptic flake ( $\omega_3 > 1 \gg \omega_2$ )

$$H_3^{\Omega} = \frac{\omega_2}{\omega_3^2 - 1} \{ F(k) - E(k) \} , \quad H_1^{\Omega} = -\frac{\omega_2}{\omega_3^2 - 1} \{ F(k) - \omega_3^2 E(k) \} , \quad H_2^{\Omega} = 1 - \omega_2 E(k) ,$$

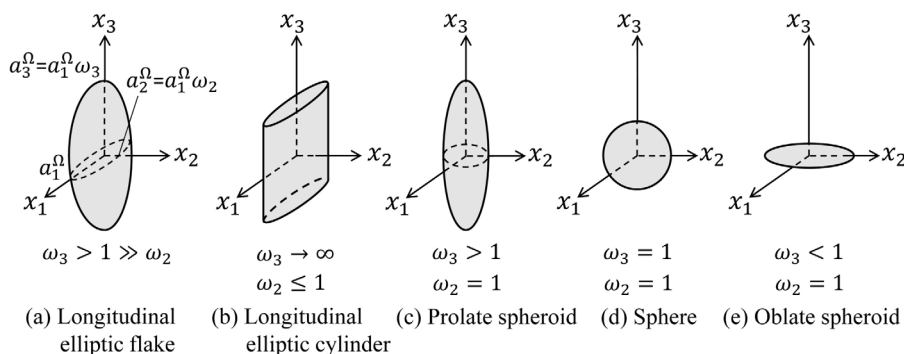


Fig. A.1. Various shapes of ellipsoidal filler.

$$H_{23}^{\Omega} = H_2^{\Omega} - H_3^{\Omega} \quad , \quad H_{31}^{\Omega} = \frac{1}{\omega_3^2 - 1} (H_1^{\Omega} - H_3^{\Omega}) , \quad (\text{A.4a})$$

(b) Longitudinal elliptic cylinder ( $\omega_3 \rightarrow \infty$ ,  $\omega_2 \leq 1$ )

$$H_1^{\Omega} = \frac{\omega_2}{1 + \omega_2} \quad , \quad H_2^{\Omega} = H_{23}^{\Omega} = \frac{1}{1 + \omega_2} \quad , \quad H_{12}^{\Omega} = \frac{\omega_2^2}{(1 + \omega_2)^2} , \quad (\text{A.4b})$$

(c) Prolate spheroid ( $\omega_3 > 1$ ,  $\omega_2 = 1$ )

$$\begin{aligned} H_3^{\Omega} &= 1 - \frac{\omega_3}{(\omega_3^2 - 1)^{3/2}} \{ \omega_3 (\omega_3^2 - 1)^{1/2} - \cosh^{-1} \omega_3 \} \quad , \quad H_1^{\Omega} = H_2^{\Omega} = \frac{1}{2} (1 - H_3^{\Omega}) , \\ H_{12}^{\Omega} &= \frac{1}{4} (1 - H_{31}^{\Omega}) \quad , \quad H_{23}^{\Omega} = \frac{1}{2} (1 - 3H_3^{\Omega}) + H_{31}^{\Omega} = \omega_3^2 H_{31}^{\Omega} , \\ H_{31}^{\Omega} &= \frac{1 - 3H_3^{\Omega}}{2(\omega_3^2 - 1)} = \frac{H_1^{\Omega} - H_3^{\Omega}}{\omega_3^2 - 1} , \end{aligned} \quad (\text{A.4c})$$

(d) Sphere ( $\omega_3 = \omega_2 = 1$ )

$$H_3^{\Omega} = H_1^{\Omega} = H_2^{\Omega} = \frac{1}{3} \quad , \quad H_{12}^{\Omega} = H_{23}^{\Omega} = H_{31}^{\Omega} = \frac{1}{5} , \quad (\text{A.4d})$$

(e) oblate spheroid ( $\omega_3 < 1$ ,  $\omega_2 = 1$ )

$$\begin{aligned} H_3^{\Omega} &= 1 - \frac{\omega_3}{(1 - \omega_3^2)^{3/2}} \{ \cos^{-1} \omega_3 - \omega_3 (1 - \omega_3^2)^{1/2} \} \quad , \quad H_1^{\Omega} = H_2^{\Omega} = \frac{1}{2} (1 - H_3^{\Omega}) , \\ H_{12}^{\Omega} &= \frac{1}{4} (1 - H_{31}^{\Omega}) \quad , \quad H_{23}^{\Omega} = \frac{1}{2} (1 - 3H_3^{\Omega}) + H_{31}^{\Omega} = \omega_3^2 H_{31}^{\Omega} , \\ H_{31}^{\Omega} &= -\frac{1 - 3H_3^{\Omega}}{2(1 - \omega_3^2)} = \frac{H_1^{\Omega} - H_3^{\Omega}}{\omega_3^2 - 1} . \end{aligned} \quad (\text{A.4e})$$

$F(k)$  and  $E(k)$  are complete elliptic integrals of the first and second kinds, and  $k$  is given by

$$k = \left( \frac{\omega_3^2 - 1}{\omega_3^2} \right)^{1/2} . \quad (\text{A.5})$$

## A.2. Coefficients appearing in equations of equivalent eigenstrains

The coefficients  $D_I$  to  $D_V$  and  $D^{\Sigma}$  appearing in equations of equivalent eigenstrains obtained in Section 2 represent invariants that do not depend on the coordinate system. They are given by

$$\begin{aligned} D_I &= L_I D_{II} - 2(1 - 2\bar{\nu}) D_V \quad , \quad D_{II} = (D_{IV})^2 - \frac{3}{2} \sum_{i=1}^3 (R_i)^2 , \\ D_{III} &= L_I D_{IV} - \frac{1}{9} (1 + \bar{\nu})(1 - 2\bar{\nu}) \sum_{i=1}^3 (\alpha_i)^2 \quad , \quad D_{IV} = L_{II} + H_I - 1 , \\ D_V &= \frac{1}{9} (1 + \bar{\nu}) \sum_{i=1}^3 \alpha_i G_i \quad , \quad D^{\Sigma} = \sum_{i=1}^3 \frac{1}{D_{IV} + S_i} , \end{aligned} \quad (\text{A.6})$$

where  $L_I$  and  $L_{II}$  include the bulk modulus and the shear modulus of constituents, and are given as follows:

$$L_I = 3(1 - \bar{\nu})L_K - 2(1 - 2\bar{\nu}) \quad , \quad L_{II} = 2(1 - \bar{\nu})L_{\mu} - \frac{1}{3}(1 - 2\bar{\nu}) , \quad (\text{A.7})$$

$$L_K = \frac{K^{\Omega}}{K^{\Omega} - \bar{K}} \quad , \quad L_{\mu} = \frac{\mu^{\Omega}}{\mu^{\Omega} - \bar{\mu}} . \quad (\text{A.8})$$

The component-dependent coefficients  $F_i$ ,  $G_i$ ,  $\alpha_i$ ,  $\beta_i$ ,  $R_i$ , and  $S_i$  are given by

$$F_1 = \frac{2}{3} (1 + \bar{\nu})(1 - 2\bar{\nu}) \left\{ (\alpha_1)^2 - \frac{1}{3} \sum_{i=1}^3 (\alpha_i)^2 \right\} + 3L_I R_1 , \quad (\text{A.9a})$$

$$G_1 = \alpha_1 (D_{IV} + 3R_1) - \sum_{i=1}^3 \alpha_i R_i , \quad (\text{A.9b})$$

$$\alpha_1 = 1 - 3H_1^{\Omega} \quad , \quad \beta_1 = H_2^{\Omega} - H_{23}^{\Omega} , \quad (\text{A.10a})$$

$$R_1 = \frac{2}{9} (1 - 2\bar{\nu}) \alpha_1 + \beta_1 - \frac{1}{3} H_1 \quad , \quad S_1 = \frac{2}{3} (1 - \bar{\nu}) \alpha_1 - 2\beta_1 - H_1 + \frac{2}{3} \quad , \quad H_1 = \sum_{i=1}^3 \beta_i . \quad (\text{A.10b})$$

The other components 2 and 3 are obtained by circularly permuting subscripts.

## A.3. Matrix of coordinate transformation

Fig. A.2 shows the spherical coordinate system expressed by Euler angles, where  $\theta$ ,  $\phi$  and  $\psi$  are the zenith, azimuth, and rotation angles of a filler. In the case of the y-convention, the coordinate transformation is performed by first rotating an azimuth angle  $\phi$  around the  $z$ -axis, then a

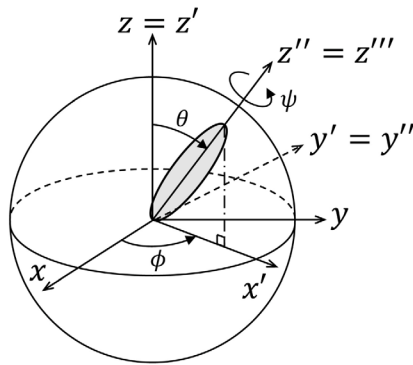


**Fig. A.2.** Spherical coordinate system expressed by Euler angles.

zenith angle  $\theta$  around the  $y$ -axis, and finally a rotation angle  $\psi$  around the  $z$ -axis again. The matrix of coordinate transformation in the  $y$ -convention  $l$  is given by Toda [29],

$$l = \begin{bmatrix} l_{11} & l_{12} & l_{13} \\ l_{21} & l_{22} & l_{23} \\ l_{31} & l_{32} & l_{33} \end{bmatrix} = \begin{bmatrix} \cos \psi & \sin \psi & 0 \\ -\sin \psi & \cos \psi & 0 \\ 0 & 0 & 1 \end{bmatrix} \begin{bmatrix} \cos \theta & 0 & -\sin \theta \\ 0 & 1 & 0 \\ \sin \theta & 0 & \cos \theta \end{bmatrix} \begin{bmatrix} \cos \phi & \sin \phi & 0 \\ -\sin \phi & \cos \phi & 0 \\ 0 & 0 & 1 \end{bmatrix} \\ = \begin{bmatrix} \cos \theta \cos \phi \cos \psi - \sin \phi \sin \psi & \cos \theta \sin \phi \cos \psi + \cos \phi \sin \psi & -\sin \theta \cos \psi \\ -\cos \theta \cos \phi \sin \psi - \sin \phi \cos \psi & -\cos \theta \sin \phi \sin \psi + \cos \phi \cos \psi & \sin \theta \sin \psi \\ \sin \theta \cos \phi & \sin \theta \sin \phi & \cos \theta \end{bmatrix}. \quad (\text{A.11})$$

The matrices of coordinate transformation  $L$  and  $\hat{L}$  used in Eq. (12) are expressed as

$$L = \begin{bmatrix} \frac{1}{3}L^\Sigma & L_1^{\Sigma'} & L_2^{\Sigma'} & L_3^{\Sigma'} & 2L_{23}^{\Sigma'} & 2L_{31}^{\Sigma'} & 2L_{12}^{\Sigma'} \\ \frac{1}{3}(L_1^\Sigma - \frac{L^\Sigma}{3}) & l_{11}^2 - \frac{L_1^{\Sigma'}}{3} & l_{12}^2 - \frac{L_2^{\Sigma'}}{3} & l_{13}^2 - \frac{L_3^{\Sigma'}}{3} & 2(l_{12}l_{13} - \frac{L_{23}^{\Sigma'}}{3}) & 2(l_{13}l_{11} - \frac{L_{31}^{\Sigma'}}{3}) & 2(l_{11}l_{12} - \frac{L_{12}^{\Sigma'}}{3}) \\ \frac{1}{3}(L_2^\Sigma - \frac{L^\Sigma}{3}) & l_{21}^2 - \frac{L_1^{\Sigma'}}{3} & l_{22}^2 - \frac{L_2^{\Sigma'}}{3} & l_{23}^2 - \frac{L_3^{\Sigma'}}{3} & 2(l_{22}l_{23} - \frac{L_{23}^{\Sigma'}}{3}) & 2(l_{23}l_{21} - \frac{L_{31}^{\Sigma'}}{3}) & 2(l_{21}l_{22} - \frac{L_{12}^{\Sigma'}}{3}) \\ \frac{1}{3}(L_3^\Sigma - \frac{L^\Sigma}{3}) & l_{31}^2 - \frac{L_1^{\Sigma'}}{3} & l_{32}^2 - \frac{L_2^{\Sigma'}}{3} & l_{33}^2 - \frac{L_3^{\Sigma'}}{3} & 2(l_{32}l_{33} - \frac{L_{23}^{\Sigma'}}{3}) & 2(l_{33}l_{31} - \frac{L_{31}^{\Sigma'}}{3}) & 2(l_{31}l_{32} - \frac{L_{12}^{\Sigma'}}{3}) \\ \frac{1}{3}L_{23}^\Sigma & l_{21}l_{31} & l_{22}l_{32} & l_{23}l_{33} & l_{22}l_{33} + l_{32}l_{23} & l_{23}l_{31} + l_{33}l_{21} & l_{21}l_{32} + l_{31}l_{22} \\ \frac{1}{3}L_{31}^\Sigma & l_{31}l_{11} & l_{32}l_{12} & l_{33}l_{13} & l_{32}l_{13} + l_{12}l_{33} & l_{33}l_{11} + l_{13}l_{31} & l_{31}l_{12} + l_{11}l_{32} \\ \frac{1}{3}L_{12}^\Sigma & l_{11}l_{21} & l_{12}l_{22} & l_{13}l_{23} & l_{12}l_{23} + l_{22}l_{13} & l_{13}l_{21} + l_{23}l_{11} & l_{11}l_{22} + l_{21}l_{12} \end{bmatrix}, \quad (\text{A.12a})$$

$$\hat{L} = \begin{bmatrix} \frac{1}{3}L^\Sigma & L_1^\Sigma & L_2^\Sigma & L_3^\Sigma & 2L_{23}^\Sigma & 2L_{31}^\Sigma & 2L_{12}^\Sigma \\ \frac{1}{3}(L_1^\Sigma - \frac{L^\Sigma}{3}) & l_{11}^2 - \frac{L_1^\Sigma}{3} & l_{21}^2 - \frac{L_2^\Sigma}{3} & l_{31}^2 - \frac{L_3^\Sigma}{3} & 2(l_{21}l_{31} - \frac{L_{23}^\Sigma}{3}) & 2(l_{31}l_{11} - \frac{L_{31}^\Sigma}{3}) & 2(l_{11}l_{21} - \frac{L_{12}^\Sigma}{3}) \\ \frac{1}{3}(L_2^\Sigma - \frac{L^\Sigma}{3}) & l_{12}^2 - \frac{L_1^\Sigma}{3} & l_{22}^2 - \frac{L_2^\Sigma}{3} & l_{32}^2 - \frac{L_3^\Sigma}{3} & 2(l_{22}l_{32} - \frac{L_{23}^\Sigma}{3}) & 2(l_{32}l_{12} - \frac{L_{31}^\Sigma}{3}) & 2(l_{12}l_{22} - \frac{L_{12}^\Sigma}{3}) \\ \frac{1}{3}(L_3^\Sigma - \frac{L^\Sigma}{3}) & l_{13}^2 - \frac{L_1^\Sigma}{3} & l_{23}^2 - \frac{L_2^\Sigma}{3} & l_{33}^2 - \frac{L_3^\Sigma}{3} & 2(l_{23}l_{33} - \frac{L_{23}^\Sigma}{3}) & 2(l_{33}l_{13} - \frac{L_{31}^\Sigma}{3}) & 2(l_{13}l_{23} - \frac{L_{12}^\Sigma}{3}) \\ \frac{1}{3}L_{23}^\Sigma & l_{12}l_{13} & l_{22}l_{23} & l_{32}l_{33} & l_{22}l_{33} + l_{23}l_{32} & l_{32}l_{13} + l_{33}l_{12} & l_{12}l_{23} + l_{13}l_{22} \\ \frac{1}{3}L_{31}^\Sigma & l_{13}l_{11} & l_{23}l_{21} & l_{33}l_{31} & l_{23}l_{31} + l_{21}l_{33} & l_{33}l_{11} + l_{31}l_{13} & l_{13}l_{21} + l_{11}l_{23} \\ \frac{1}{3}L_{12}^\Sigma & l_{11}l_{12} & l_{21}l_{22} & l_{31}l_{32} & l_{21}l_{32} + l_{22}l_{31} & l_{31}l_{12} + l_{32}l_{11} & l_{11}l_{22} + l_{12}l_{21} \end{bmatrix}, \quad (\text{A.12b})$$

where

$$L^\Sigma = L_1^\Sigma + L_2^\Sigma + L_3^\Sigma = L_1^{\Sigma'} + L_2^{\Sigma'} + L_3^{\Sigma'}, \\ L_1^\Sigma = l_{11}^2 + l_{12}^2 + l_{13}^2, \quad L_2^\Sigma = l_{21}^2 + l_{22}^2 + l_{23}^2, \quad L_3^\Sigma = l_{31}^2 + l_{32}^2 + l_{33}^2, \\ L_1^{\Sigma'} = l_{11}^2 + l_{21}^2 + l_{31}^2, \quad L_2^{\Sigma'} = l_{12}^2 + l_{22}^2 + l_{32}^2, \quad L_3^{\Sigma'} = l_{13}^2 + l_{23}^2 + l_{33}^2, \\ L_{23}^\Sigma = l_{21}l_{31} + l_{22}l_{32} + l_{23}l_{33}, \quad L_{31}^\Sigma = l_{31}l_{11} + l_{32}l_{12} + l_{33}l_{13}, \quad L_{12}^\Sigma = l_{11}l_{21} + l_{12}l_{22} + l_{13}l_{23}, \\ L_{23}^{\Sigma'} = l_{12}l_{13} + l_{22}l_{23} + l_{32}l_{33}, \quad L_{31}^{\Sigma'} = l_{13}l_{11} + l_{23}l_{21} + l_{33}l_{31}, \quad L_{12}^{\Sigma'} = l_{11}l_{12} + l_{21}l_{22} + l_{31}l_{32}. \quad (\text{A.13})$$

## References

- [1] S. Kari, H. Berger, U. Gabbert, Numerical evaluation of effective material properties of randomly distributed short cylindrical fibre composites, *Comput. Mater. Sci.* 39 (2007) 198–204, <http://dx.doi.org/10.1016/j.commatsci.2006.02.024>.
- [2] B. Wang, R. Wang, Y. Wu, The Young's moduli prediction of random distributed short-fiber-reinforced polypropylene foams using finite element method, *Sci. China Ser. E: Technol. Sci.* 52 (2009) 72–78, <http://dx.doi.org/10.1007/s11431-008-0282-7>.

- [3] F.E. El-Abbassi, M. Assarar, S. Sakami, H. Kebir, R. Ayad, The effect of micromechanics models: 2D and 3D numerical modeling for predicting the mechanical properties of PP/Alfa short fiber composites, *J. Compos. Sci.* 6 (2022) 1–10, <http://dx.doi.org/10.3390/jcs6030066>.
- [4] T.-D. Nguyen, N.D. Duc, Evaluation of elastic properties and thermal expansion coefficient of composites reinforced by randomly distributed spherical particles with negative Poisson's ratio, *Compos. Struct.* 153 (2016) 569–577, <http://dx.doi.org/10.1016/j.comstruct.2016.06.069>.
- [5] W. Tian, L. Qi, J. Liang, X. Chao, J. Zhou, Evaluation for elastic properties of metal matrix composites with randomly distributed fibers: Two-step mean-field homogenization procedure versus FE homogenization method, *J. Alloys Compd.* 658 (2016) 241–247, <http://dx.doi.org/10.1016/j.jallcom.2015.10.190>.
- [6] Z. Hashin, S. Shtrikman, A variational approach to the theory of the elastic behavior of multiphase materials, *J. Mech. Phys. Solids* 11 (1963) 127–140, [http://dx.doi.org/10.1016/0022-5096\(63\)90060-7](http://dx.doi.org/10.1016/0022-5096(63)90060-7).
- [7] R.M. Christensen, F.M. Walls, Effective stiffness of randomly oriented fibre composites, *J. Compos. Mater.* 6 (1972) 518–532, <http://dx.doi.org/10.1177/002199837200600307>.
- [8] R.M. Christensen, *Mechanics of Composite Materials*, Dover publications, 2005, pp. 106–151.
- [9] T. Mori, K. Tanaka, Average stress in matrix and average elastic energy of materials with misfitting inclusions, *Acta Metall.* 21 (1973) 571–574, [http://dx.doi.org/10.1016/0001-6160\(73\)90064-3](http://dx.doi.org/10.1016/0001-6160(73)90064-3).
- [10] B. Budiansky, On the elastic moduli of some heterogeneous materials, *J. Mech. Phys. Solids* 13 (1965) 223–227, [http://dx.doi.org/10.1016/0022-5096\(65\)90011-6](http://dx.doi.org/10.1016/0022-5096(65)90011-6).
- [11] S. Nemat-Nasser, M. Hori, *Micromechanics : Overall Properties of Heterogeneous Materials*, North-Holland, 1993, pp. 329–340.
- [12] G. Huang, Some closed-form solutions for effective moduli of composites containing randomly oriented short fibers, *Mater. Sci. Eng. A* 315 (2001) 11–20, [http://dx.doi.org/10.1016/S0921-5093\(01\)01212-6](http://dx.doi.org/10.1016/S0921-5093(01)01212-6).
- [13] T.T. Wu, The effect of inclusion shape on the elastic moduli of a two-phase material, *Int. J. Solids Struct.* 2 (1966) 1–8, [http://dx.doi.org/10.1016/0020-7683\(66\)90002-3](http://dx.doi.org/10.1016/0020-7683(66)90002-3).
- [14] V.-L. Nguyen, FFT, DA, and mori-tanaka approximation to determine the elastic moduli of three-phase composites with the random inclusions, *EPJ Appl. Math.* 9 (2022) 1–8, <http://dx.doi.org/10.1051/epjam/2022007>.
- [15] T. Mura, *Micromechanics of Defects in Solids Second Revised Edition*, KLUWER ACADEMIC PUBLISHERS, 1987, pp. 177–187.
- [16] G.P. Tandon, G.J. Weng, Average stress in the matrix and effective moduli of randomly oriented composites, *Compos. Sci. Technol.* 27 (1986) 111–132, [http://dx.doi.org/10.1016/0266-3538\(86\)90067-9](http://dx.doi.org/10.1016/0266-3538(86)90067-9).
- [17] J. Luo, R. Stevens, Micromechanics of randomly oriented ellipsoidal inclusion composite. Part I: Stress, strain and thermal expansion, *J. Appl. Phys.* 79 (1996) 9047–9056, <http://dx.doi.org/10.1063/1.362638>.
- [18] J. Luo, R. Stevens, Micromechanics of randomly oriented ellipsoidal inclusion composite. Part II: Elastic moduli, *J. Appl. Phys.* 79 (1996) 9057–9063, <http://dx.doi.org/10.1063/1.362639>.
- [19] B. Raju, S.R. Hiremath, D.R. Mahapatra, A review of micromechanics based models for effective elastic properties of reinforced polymer matrix composites, *Compos. Struct.* 204 (2018) 607–619, <http://dx.doi.org/10.1016/j.compstruct.2018.07.125>.
- [20] S. Araki, H. Yamashita, H. Ono, Effect of change in shape of ellipsoidal reinforcement on macroscopic elastic moduli of a composite material, *Trans. JSME (in Japanese)* 75 (760) (2009) 1702–1709, <http://dx.doi.org/10.1299/kikaia.75.1702>.
- [21] K. Takahashi, T. Kobayashi, K. Kitagawa, K. Harakawa, K. Tanaka, Experimental study on the Young's modulus of particulate reinforced epoxy-resin using model specimens, *J. Soc. Mater. Sci. Japan* 27 (293) (1978) 183–188, <http://dx.doi.org/10.2472/jsms.27.183>.
- [22] K. Okuno, On the flexural modulus of the flake-filled plastics, *Kobunshi Ronbunshu (in Japanese)* 37 (1980) 789–796, <http://dx.doi.org/10.1295/koron.37.789>.
- [23] M. Miwa, T. Ohsawa, Y. Ando, K. Sako, Thermal expansion behavior for the short glass fiber-epoxy composite and the short glass fiber-unsaturated polyester composite, *Sen'i Gakkaishi (in Japanese)* 36 (1980) 7–13, <http://dx.doi.org/10.2115/fiber.36.T7>.
- [24] N.A. Farrah, J. Mariatti, P. Samayamuthirian, A.M.A. Khairun, Effect of particle shape of silica mineral on the properties of epoxy composites, *Compos. Sci. Technol.* 68 (2008) 346–353, <http://dx.doi.org/10.1016/j.compscitech.2007.07.015>.
- [25] A. Bouti, T. Vu-Khanh, B. Fisa, Injection molding of glass flake reinforced polypropylene: Flake orientation and stiffness, *Polym. Compos.* 10 (5) (1989) 352–359, <http://dx.doi.org/10.1002/pc.750100512>.
- [26] B.W. Rosen, Z. Hashin, Effective thermal expansion coefficients and specific heats of composite materials, *Int. J. Eng. Sci.* 8 (1970) 157–173, [http://dx.doi.org/10.1016/0020-7225\(70\)90066-2](http://dx.doi.org/10.1016/0020-7225(70)90066-2).
- [27] S. Kanaun, V. Levin, *Self-Consistent Methods for Composites Volume 1-Static Problems*, Springer, 1986, pp. 281–287.
- [28] S. Li, G. Wang, *Introduction to Micromechanics and Nanomechanics*, World Scientific Publishing Co., 2008, pp. 131–158.
- [29] M. Toda, *Classical Mechanics(an Introductory Course of Physics 1)*, Iwanami Shoten, 2002, pp. 205–206.